J|A|C|S ARTICLES

Published on Web 05/04/2009

The Emergence of Nonbulk Properties in Supported Metal Clusters: Negative Thermal Expansion and Atomic Disorder in Pt Nanoclusters Supported on γ-Al_2O_3

Sergio I. Sanchez,[†] Laurent D. Menard,[†] Ariella Bram,[‡] Joo H. Kang,[†] Matthew W. Small,[†] Ralph G. Nuzzo,*[,†] and Anatoly I. Frenkel*[,‡]

School of Chemical Sciences and the Frederick Seitz Materials Research Laboratory, University of Illinois, Urbana, Illinois 61801, and the Department of Physics, Yeshiva University, New York, New York 10016

Received November 25, 2008; E-mail: r-nuzzo@illinois.edu; anatoly.frenkel@yu.edu

Abstract: The structural dynamics−cluster size and adsorbate-dependent thermal behaviors of the metal−metal (M−M) bond distances and interatomic order−of Pt nanoclusters supported on a γ-Al_2O_3 are described. Data from scanning transmission electron microscopy (STEM) and X-ray absorption spectroscopy (XAS) studies reveal that these materials possess a dramatically nonbulklike nature. Under an inert atmosphere small, subnanometer Pt/γ-Al_2O_3 clusters exhibit marked relaxations of the M−M bond distances, negative thermal expansion (NTE) with an average linear thermal expansion coefficient $\alpha = (-2.4 \pm 0.4) \times 10^{-5}$ K^{-1}, large static disorder and dynamical bond (interatomic) disorder that is poorly modeled within the constraints of classical theory. The data further demonstrate a significant temperature-dependence to the electronic structure of the Pt clusters, thereby suggesting the necessity of an active model to describe the cluster/support interactions mediating the cluster's dynamical structure. The quantitative dependences of these nonbulklike behaviors on cluster size (0.9 to 2.9 nm), ambient atmosphere (He, 4% H_2 in He or 20% O_2 in He) and support identity (γ-Al_2O_3 or carbon black) are systematically investigated. We show that the nonbulk structural, electronic and dynamical perturbations are most dramatically evidenced for the smallest clusters. The adsorption of hydrogen on the clusters leads to an increase of the Pt−Pt bondlengths (due to a lifting of the surface relaxation) and significant attenuation of the disorder present in the system. Oxidation of these same clusters has the opposite effect, leading to an increase in Pt−Pt bond strain and subsequent enhancement in nonbulklike thermal properties. The structural and electronic properties of Pt nanoclusters supported on carbon black contrast markedly with those of the Pt/γ-Al_2O_3 samples in that neither NTE nor comparable levels of atomic disorder are observed. The Pt/C nanoclusters do exhibit, however, both size- and adsorbate-induced trends in bond strain that are similar to those of their Pt/γ-Al_2O_3 analogues. Taken together, the data highlight the significant role that electronic effects − specifically charge exchange due to both metal−support and metal−adsorbate interactions − play in mediating the structural dynamics of supported nanoscale metal clusters that are broadly used as heterogeneous catalysts.

1. Introduction

Supported metal clusters are widely used as catalysts, finding application in diverse technologies that are critical to the growth of the American economy.[1−3] Prominent examples of processes in which supported metal catalysts play an indispensable role include petroleum refining,[2,3] environmental remediation (e.g., automotive exhaust stream processing),[4,5] chemical synthesis,[3,6] and fuel-cell-based power generation.[7−10] Materials of this type are inherently complex systems where the activity and selectivity are determined by the chemical and structural nature of catalytically active surface sites.[4,11,12]

One critical parameter that influences the characteristics of the surface sites present on a metal cluster is its size. A decrease in the cluster size results in geometrical changes (e.g., the relative areas of exposed (100) and (111) surface facet planes)

[†] University of Illinois at Urbana−Champaign.
[‡] Yeshiva University.

(1) Rase, H. F. *Handbook of Commercial Catalysts: Heterogeneous Catalysts*; CRC Press: Boca Raton, 2000.
(2) Satterfield, C. N. *Heterogeneous Catalysis in Industrial Practice*, 2nd ed.; McGraw-Hill, Inc.: New York, 1991.
(3) Gates, B. C. *Catalytic Chemistry*; John Wiley & Sons, Inc.: New York, 1992.
(4) Sinfelt, J. H. *Bimetallic Catalysts: Discoveries, Concepts and Applications*; Wiley: New York, 1983.
(5) Gandhi, H. S.; Graham, G. W.; McCabe, R. W. *J. Catal.* **2003**, *216*, 433–442.
(6) Raja, R.; Khimyak, T.; Thomas, J. M.; Hermans, S.; Johnson, B. F. G. *Angew. Chem., Int. Ed.* **2001**, *40* (24), 4638–4642.
(7) Thomas, J. M.; Raja, R.; Johnson, B. F. G.; Hermans, S.; Jones, M. D.; Khimyak, T. *Ind. Eng. Chem. Res.* **2003**, *42*, 1563–1570.
(8) Li, H.; Sun, G.; Li, N.; Sun, S.; Su, D.; Xin, Q. *J. Phys. Chem. C* **2007**, *111*, 5605–5617.
(9) Wen, F.; Simon, U. *Chem. Mater.* **2007**, *19*, 3370–3372.
(10) Min, M.-K.; Cho, J.; Cho, K.; Kim, H. *Electrochim. Acta* **2000**, *45*, 4211–4217.
(11) Bernard, C.; Figueras, F. *Coord. Chem. Rev.* **1998**, *178−180*, 1753–1783.
(12) Henry, C. R. *Surf. Sci. Rep.* **1998**, *31*, 231–325.

 10.1021/ja809182v CCC: $40.75

and, perhaps equally important, changes in its corresponding electronic structure.[3,11−13] These perturbations are expressed most dramatically at the smallest particle sizes, a fact that has motivated numerous studies that have managed to characterize such materials in a variety of contexts down to subnanometer dimensions.[14−17]Studies that have focused on catalytic activity as a function of nanoparticle size typically find correlations that are highly reaction dependent. Au, while essentially inert in its bulk form, shows significant activity for CO oxidation when dispersed as a nanoparticle on an appropriate support.[18−20] In a model Au/TiO_2(001) system, for example, the activity for CO oxidation varies with cluster size and peaks at a cluster diameter of ∼3 nm.[21] In contrast, the activity of Pt/C nanoparticles in the electrochemical oxygen reduction reaction was recently reported to show no significant dependence on nanoparticle size, save perhaps for that due to surface area effects.[22] Current literature paints a complex story as to how metal particle sizes influence the diverse range of properties that are central to catalytic efficiency in real process applications−notable among these are sensitivities related to poisoning or deactivation,[2,3,23,24] stability against sintering,[2,3,25,26] and the efficacy of regeneration.[2,3,27−29] In such contexts, understanding contributions to structure−property correlations associated with the nature of the metal−support interactions remains among the most important and, as of yet, incompletely developed aspects of the problem.[30−35] Questions such as the precise atomistic nature of the bonding that governs these interactions, and the impacts that follow for the electronic structure and structural dynamics of supported metallic clusters, comprise what are perhaps the most difficult problems in the field.

The catalytic behaviors of very small clusters, systems where the electronic and structural consequences of the support interaction would be most heavily weighted, are expected to show pronounced sensitivity to the nature of the metal−support bonding.[30−35] The present work addresses itself to structural, dynamic, and electronic features exhibited in a highly prototypical catalytic system of this type: Pt clusters supported on γ-Al_2O_3. This material is a heterogeneous catalyst used in the processes that produce essentially all the liquid hydrocarbon fuels consumed worldwide.[2,3] This report follows and expands upon an earlier study that demonstrated the surprising onset of nonbulklike mesoscopic structural behaviors in this system at nanometer particle sizes.[17] That work suggested that the support interactions are not "passive," but instead convolve electronic effects that significantly perturb the atomic structure of the clusters. We present results that define dramatic, and in some respect nonintuitive, chemical sensitivities of the structural behaviors seen in this system. These results include the occurrence of negative thermal expansion (NTE) in the M−M Pt bond distances, as well as the impacts of nanoparticle size (average sizes of 0.9 ± 0.2, 1.1 ± 0.3, and 2.9 ± 0.9 nm) and the presence of either reactive (H_2, O_2) or inert (He) atmospheres. Our findings illustrate which trends are size- and adsorbate-dependent and further confirm the importance of charge transfer in describing the emergent mesoscopic behaviors of the Pt/γ-Al_2O_3 system.

2. Experimental Methods

2.1. Preparation of Supported Pt Clusters. Pt clusters were prepared on γ-Al_2O_3 (Aldrich, surface area 220 m^2/g) by impregnating the Pt^{2+} precursor, $Pt(NH_3)_4(OH)_2 \cdot H_2O$ (Strem Chemicals, Inc.), onto the support from an aqueous solution using the incipient wetness method to yield a Pt weight loading of 1%. The supported precursor was dried under vacuum, pressed into a pellet, and mounted in an *in situ* XAS cell. The sample was heated under a stream of H_2 (4% in He) to a final temperature of 573 K to remove the ligands and reduce the precursor to metallic clusters. This resulted in a final average cluster size of 0.9 nm. In order to obtain a slightly larger average cluster size (1.1 nm) a second pellet of the supported precursor was subjected to a similar treatment, except a final reduction temperature of 687 K was used. A third, commercial Pt on γ-Al_2O_3 sample with an average particle size of 2.9 nm and a weight loading of 5% (Sigma-Aldrich) was also pressed into a pellet from the commercial powder and activated under H_2 flow at 573 K prior to taking XAS measurements.

Small Pt clusters on carbon black (Cabot, Vulcan XC72, surface area 250 m^2/g) were prepared in a similar manner from the $Pt(NH_3)_4(OH)_2 \cdot H_2O$ precursor, followed by reduction under H_2 at 450 K, to yield clusters with an average diameter of 1.0 nm and a Pt weight loading of 1%. Commercial Pt nanoparticles supported on carbon black (XC72) with an average particle size of 1.8 nm and a 10% weight loading (ETEK, Inc.) were also pressed into pellets and activated by reduction under H_2 flow at 573 K prior to XAS measurements. The reduction process for all samples described above was monitored by scanning the Pt L_3 absorption edge.

2.2. Particle Size Determination and Atom Quantification Using Scanning Transmission Electron Microscopy (STEM). The samples for STEM were prepared by suspending the supported Pt particles in acetone and placing a drop of the suspensions on copper grids coated with an ultrathin carbon film on holey carbon (Ted Pella, Inc.). Dark-field images were obtained on a JEOL 2010F (S)TEM operating at 200 kV with an electron probe focused to 0.5 nm. The images were analyzed using Digital Micrograph (Gatan,

(13) Schmid, G. *Nanoparticles: From Theory to Application*; Wiley-VCH: Weinheim, 2004.
(14) Sun, Y.; Zhuang, L.; Lu, J.; Hong, X.; Liu, P. *J. Am. Chem. Soc.* **2007**, *129*, 15465–15467.
(15) Menard, L. D.; Xu, H.; Gao, S.-P.; Twesten, R. D.; Harper, A. S.; Song, Y.; Wang, G.; Douglas, A. D.; Yang, J. C.; Frenkel, A. I.; Murray, R. W.; Nuzzo, R. G. *J. Phys. Chem. B* **2006**, *30*, 14564–14573.
(16) Alexeev, O.; Gates, B. C. *Top. Catal.* **2000**, *10*, 273–293.
(17) Kang, J. H.; Menard, L. D.; Nuzzo, R. G.; Frenkel, A. I. *J. Am. Chem. Soc.* **2006**, *128*, 12068–12069.
(18) Haruta, M. *Chem. Record* **2003**, *3*, 75–87.
(19) Haruta, M.; Yamada, N.; Kobayashi, T.; Iijima, S. *J. Catal.* **1989**, *115*, 301.
(20) Choudhary, T. V.; Goodman, D. W. *Top. Catal.* **2002**, *21* (1−3), 25–34.
(21) Valden, M.; Pak, S.; Lai, X.; Goodman, D. W. *Catal. Lett.* **1998**, *56*, 7–10.
(22) Yano, H.; Inukai, J.; Uchida, H.; Watanabe, M.; Babu, P. K.; Kobayashi, T.; Chung, J. H.; Oldfield, E.; Wieckowski, A. *Phys. Chem. Chem. Phys.* **2006**, *8*, 4932–4939.
(23) Im, J.-H.; Suh, D. J.; Park, T.-J.; Kim, K.-L. *Appl. Catal., A* **2000**, *197*, 191–200.
(24) Forzatti, P. *Catal. Today* **1999**, *52*, 165–181.
(25) Aboul-Gheit, A.; Aboul-Fotouh, S. M.; Aboul-Gheit, N. A. K. *Appl. Catal., A* **2005**, *292*, 144–153.
(26) Kanazawa, T. *Catal. Lett.* **2006**, *108*, 45–47.
(27) Fullerton, D. J.; Westwook, A. V. K.; Brydson, R.; Twigg, M. V.; Jones, J. M. *Catal. Today* **2003**, *81*, 659–671.
(28) Galisteo, F. C.; Mariscal, R.; Granados, M. L.; Fierro, J. L. G.; Daley, R. A.; Anderson, J. A. *Appl. Catal., B* **2005**, *59*, 227–233.
(29) Villegas, J. I.; Kumar, N.; Heikkila, T.; Lehto, V.-P.; Salmi, T.; Murzin, D. Y. *Chem. Eng. J* **1999**, *120*, 83–89.
(30) Koningsberger, D. C.; De Graaf, J.; Mojet, B. L.; Ramaker, D. E.; Miller, J. T. *Appl. Catal., A* **2000**, *191*, 205–220.
(31) Ealet, B.; Gillet, E. *Surf. Sci.* **1993**, *281*, 91–101.
(32) Ramaker, D. E.; de Graaf, J.; van Veen, J. A. R.; Koningsberger, D. C. *J. Catal.* **2001**, *203*, 7–17.
(33) Mojet, B. L.; Miller, J. T.; Ramaker, D. E.; Koningsberger, D. C. *J. Catal.* **1999**, *186*, 373–386.
(34) Zhang, Y.; Toebes, M. L.; van der Eerden, A.; O'Grady, W. E.; de Jong, K. P.; Koningsberger, D. C. *J. Phys. Chem. B* **2004**, *108*, 18509–18519.
(35) Ealet, B.; Gillet, E. *Surf. Sci.* **1996**, *367*, 221–230.

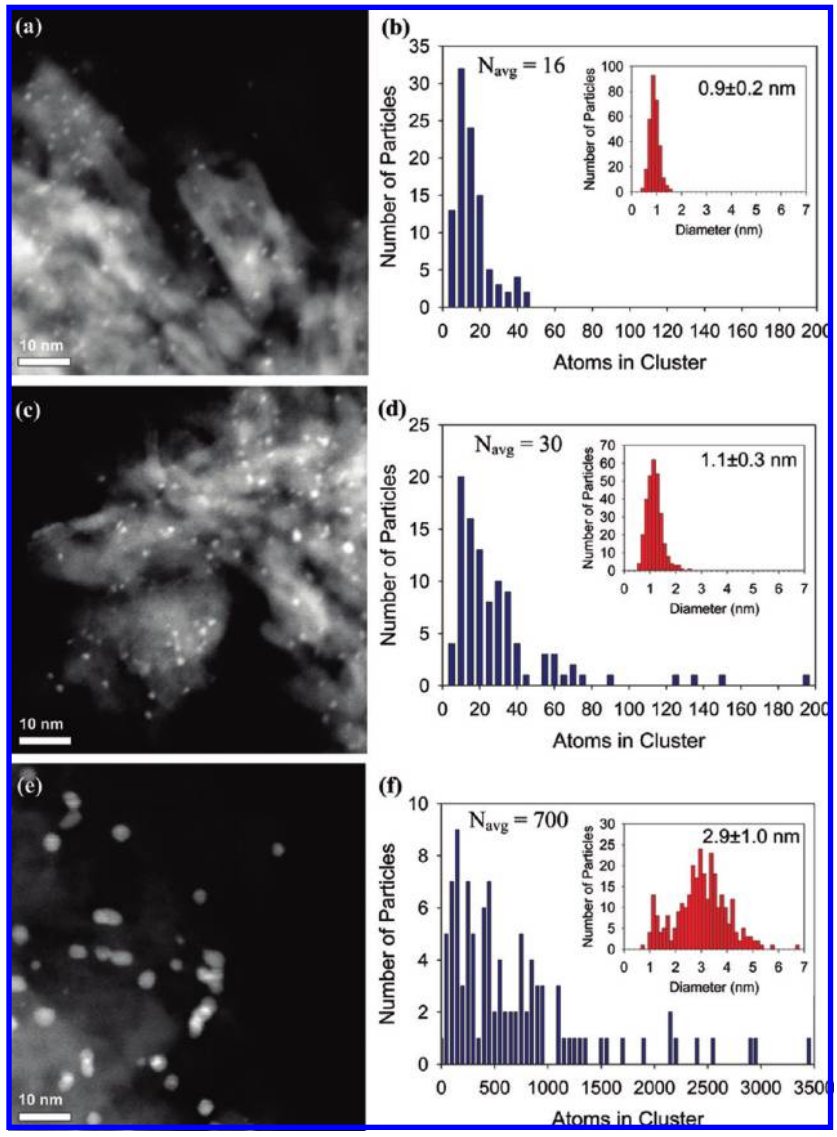

Figure 1. HAADF-STEM images and atom-count histograms shown for the (a, b) 0.9-nm, (c, d) 1.1-nm, and (e, f) 2.9-nm Pt nanoparticles supported on γ-Al_2O_3, respectively. The insets in b, d, and f are the corresponding size distribution histograms for the Pt/γ-Al_2O_3 depicted in a, c, and e.

Inc.), and the diameters of individual particles were determined from intensity profiles. The irregular intensity of the high-surface-area support materials precludes automated particle analysis routines. The error associated with measurement of the average cluster size was taken as one standard deviation (Figure 1).

Quantitative atom counting was also carried out using Digital Micrograph in the analysis of integrated areal intensities of well-isolated Pt clusters using a previously described procedure.[36] Our results indicated accurate measurements within 7% of the intensity-correlated atom counts. For instance, a calculation of a 700 atom cluster was uncertain by approximately 22 atoms for our larger clusters, while for smaller sized clusters a 16 atom cluster count was uncertain by 1 atom (Supporting Information (SI), Figure 1).

2.3. X-ray Absorption Spectroscopy. XAS measurements were performed at the XOR-UNI beamline 33BM-B at the Advanced Photon Source, Argonne National Laboratory. Some samples were also independently measured at beamline X18B at the National Synchrotron Light Source, Brookhaven National Laboratory. Results obtained at the two different synchrotrons for identical samples and experimental conditions were unchanged, within the measured uncertainties. The same *in situ* cell, suitable for experiments with low temperature (using a liquid-nitrogen-filled container with a coldfinger) and for high temperature (using a resistive heater) measurements as in our previous work[17,37] was used in these experiments. Samples were mounted at a 45° angle to the beam for spectra to be collected simultaneously in transmission and fluorescence modes. A Pt foil sample was also mounted in the beam between the transmission and reference ion chambers to collect a reference spectrum for absolute energy calibration and alignment of spectra collected from the Pt cluster samples.

Each sample was blanketed under flowing 4% H_2 in He and then heated using a variable autotransformer (Staco Energy Products, Co.) and thermocouple at the rate of 100 K/h. Upon reaching the target reduction temperature, the extent of reduction was monitored by X-ray absorption near edge structure (XANES) measurements at the Pt L_3 edge. After stabilizing the white line intensity for 30 min, full scans of the extended X-ray absorption fine structure (EXAFS) for the Pt L_3 edge were taken at a series of temperatures (165−573 K), starting at the highest temperature and then cooling and stabilizing the sample's white line intensity at successively

(36) Singhal, A.; Yang, J. C.; Gibson, J. M. *Ultramicroscopy* **1997**, *67*, 191–206.

(37) Frenkel, A. I.; Hills, C. W.; Nuzzo, R. G. *J. Phys. Chem. B* **2001**, *105*, 12689–12703.

colder temperatures. A liquid nitrogen Dewar with a coldfinger was inserted in place of the heater for subambient temperature measurements. The data were collected after the temperature stabilized to within 5 K of the lowest temperature possible, depending on the sample. Multiple scans were collected for signal averaging purposes. After completing the measurements under H_2, the gas flow was switched to ultrahigh purity He, the temperature raised, XANES scans collected and monitored until a new steady state was achieved followed by full scans made at various temperatures. At the conclusion of the measurement series, the temperature was returned to the highest value used in the series and a scan performed again to check whether the observed changes were reversible. All data presented below have passed these stringent tests of reversibility (SI, Figure 2).

These same Pt on γ-Al_2O_3 samples were then subjected to an oxygen atmosphere (leading to a partial oxidation of the clusters but with the retention of significant M−M bonding) in the *in situ* XAS cell. After complete reduction at high temperatures under 4% H_2 (as monitored by XANES), the samples were then oxidized under a flowing stream of 20% O_2, balanced by He, for one hour. In the case of the 0.9- and 1.1-nm supported cluster samples this oxidation occurred at 573 K, while the 2.9-nm commercial sample was oxidized at 673 K. The gas was switched to ultrahigh purity He at the elevated temperature followed by scanning of the XANES region. Once the XANES spectra indicated a steady state had been reached, full spectra were collected for each sample over a series of temperatures (177−573 K) from highest temperature to lowest as before. At the conclusion of these measurements, the sample was heated to the initial (highest) temperature under H_2 and a full spectrum collected to confirm the reversibility of the observed changes (SI, Figure 3).

Finally, spectra were collected from a standard Pt foil over a series of temperatures (154−700 K) similar to those used for the nanoparticle samples in order to allow a comparison of the nanoparticle dynamics and structure with bulk thermal behavior.

2.4. EXAFS Data Analysis. Data processing and analysis were performed using the IFEFFIT package, as previously described.[38,39] The spectra were aligned using the simultaneously collected Pt foil standard spectra, and the multiple scans for a given sample under identical conditions were merged. The background subtraction of the absorption edge to yield the EXAFS oscillations was performed using the AUTOBK code which implements cubic spline interpolation with an adjustable frequency cutoff to fit the background function.[40] The data were k^2-weighted and Fourier transformed to give a pseudoradial distribution function (oxidized Pt/γ-Al_2O_3 and Pt/C data were treated slightly differently, see below). The spectra were fitted in R-space by varying the coordination number (N), the photoelectron half-path length (R), the correction to the threshold energy (ΔE_0), the EXAFS Debye−Waller factor (σ^2), and the third cumulant ($\sigma^{(3)}$, which takes into account the anharmonic correction to the interatomic pair potential). Our data analysis demonstrated the significant role of anharmonic effects in the observed bond contraction and thus validated the use of the third cumulant in the data analysis. The passive electron reduction factor (S_0^2) was set to 0.86 as determined from analysis of the Pt foil spectra collected at multiple temperatures where this parameter was found to be equal to 0.86 ± 0.02. The effective scattering amplitude, phase shift and inelastic loss functions were calculated from the bulk Pt structure using a FEFF6 code.[41,42]

In order to limit the number of variables, the fitting analysis was performed simultaneously on all the spectra collected at multiple temperatures for a given sample under a given atmosphere. Furthermore, several physically reasonable constraints were made during the fitting process and will be described in greater detail in the main text. After verifying that the coordination number (N) and threshold energy correction (ΔE_0) did not vary with any statistical significance as a function of temperature (SI, Figure 4), these parameters were each fit to a single temperature-independent value across all temperatures. For all spectra, the data analysis was limited to the first-nearest-neighbor (1NN) single-scattering paths because of their isolation from longer single- and multiple-scattering paths in the Fourier-transformed spectra.

For data where a low-Z scattering contribution was present, both Pt−Pt and Pt-low-Z paths were fit using a difference file k-weighting technique.[43] Specifically, the data were weighted by k^3−to emphasize the Pt−Pt contribution and minimize errors from overlap from the Pt−O contribution−and the R-range was constrained to ∼2.1−3 Å to fit solely the Pt−Pt contribution. This best-fit theoretical contribution was then subtracted from the experimental data in k-space and the residual Pt−O contribution fit in the R-range of ∼1.4−2 Å. Theoretical standard for the Pt−O path used in the analysis of the oxidized Pt on γ-Al_2O_3 samples was calculated using a FEFF6 code from the PtO_2 structure, while that for the Pt−C path used in the analysis of the Pt on carbon black samples was calculated from a platinum carbide structure.[44,45] Because the parameters R, σ^2, and $\sigma^{(3)}$ are temperature-dependent, they were allowed to vary in the fits. No anharmonic correction was applied in the Pt-low-Z scattering path fit.[46] The thermal dependence of σ^2 was also modeled using a correlated Einstein model which represents the mean-square deviation of bond length as a superposition of static (σ_s^2) and dynamic (σ_d^2) terms:

$$\sigma^2 = \sigma_s^2 + \sigma_d^2 \tag{1}$$

$$\sigma_d^2 = \frac{\hbar}{2\omega\mu}\frac{1 + \exp(-\Theta_E/T)}{1 - \exp(-\Theta_E/T)} \tag{2}$$

where ω is the bond vibration frequency, μ is reduced mass of the absorber−scatterer pair, Θ_E is the Einstein temperature ($\Theta_E = \hbar\omega_E/k_B$), k_B is the Boltzmann's constant, and T is the measurement temperature.[47]

Representative plots for all the data and their best fits are presented as Supporting Information (SI, Figures 5−9).

3. Results

In this section we discuss the experimental results obtained using XAS (in both inert and reactive atmospheres) and STEM for Pt nanoclusters with narrow size distributions in the range of 0.9−2.9 nm supported on either γ-Al_2O_3 or carbon. High-angle annular dark-field (HAADF) STEM imaging was used to establish both the size distributions of the clusters and specific counts of metal atoms present in an average Pt cluster for each

(38) Newville, M. *J. Synchrotron Radiat.* **2001**, *8*, 322–324.
(39) Ravel, B.; Newville, M. *J. Synchrotron Radiat.* **2005**, *12*, 537–541.
(40) Newville, M.; Livins, P.; Yacoby, Y.; Rehr, J. J.; Stern, E. A. *Phys. Rev. B* **1993**, *47*, 14126–14131.
(41) Rehr, J. J.; Zabinsky, S. I.; Ankudinov, A.; Albers, R. C. *Physica B* **1995**, *208/209*, 23–26.
(42) Zabinsky, S. I.; Rehr, J. J.; Ankudinov, A. *Phys. Rev. B* **1995**, *52* (4), 2995–3009.
(43) Koningsberger, D. C.; Mojet, B. L.; van Dorssen, G. E.; Ramaker, D. E. *Top. Catal.* **2000**, *10*, 143–155.
(44) Tomaszewski, P. E. *Phase Transit* **1992**, *38*, 127–220.
(45) Ono, S.; Kikegawa, T.; Ohishi, Y. *Solid State Commun.* **2004**, *133*, 55–59.
(46) For applying an EXAFS analysis to a system with moderate bond length disorder, the anharmonicity of bond vibrations introduces a relatively small correction to the effective pair potential. To extract the lowest cumulants of the pair distribution function of a given pair requires that the EXAFS peak not overlap neighboring single- and multiple-scattering contributions. When a Pt low-Z contribution becomes significant, the Pt−Pt coordination becomes a second nearest neighbor (2NN). It is expected then that its analysis via the third cumulant may be unstable, due to the interference with Pt low-Z contribution. For such cases special caution is needed. In this work the cited difference file technique could be used to reliably isolate the third cumulants of Pt−Pt bonds in these situations.
(47) Frenkel, A. I.; Rehr, J. J. *Phys. Rev. B* **1993**, *48*, 585–588.

sample. These data provide strict constraints and points of comparison for cluster characterizations made using XAS[37] and verifies that the latter ensemble-average determinations of the local atomic environment provide a relevant atomic-level structural description of an individual cluster.[48]

3.1. Particle Size Distributions: STEM results. HAADF-STEM micrographs of three different Pt on γ-Al_2O_3 samples obtained after high-temperature reduction are shown in Figure 1. Reduction of the supported Pt^{2+} precursor at 573 K, at a loading weight of 1 wt % Pt, resulted in the smallest mean particle diameter and the narrowest size distribution—as evident from the data of Figure 1a and the inset of Figure 1b (0.9 ± 0.2 nm). Quantitative analysis of intensity maps for the individual nanoparticles in the images provided an approximate atom count contained per cluster (SI, Figure 1). Figure 1b shows that on average the number of Pt atoms contained within the 0.9-nm clusters is approximately 16 ($N_{avg} = 16$). This suggests that the structural motif of these clusters must be, in fact, an oblate rather than spherical particle.[17] Performing the reduction with the same loading at 687 K gave a larger mean particle diameter with a slightly broader width to the distribution, as seen in Figure 1c and the inset of Figure 1d (1.1 ± 0.3 nm). Quantitative analyses of the HAADF-STEM data shows that the average cluster contains a significantly larger number of Pt atoms, $N_{avg} = 30$ (Figure 1d). We also examined a commercial sample, 5% Pt on γ-Al_2O_3, and found that it exhibited the largest and broadest distribution of particle sizes, 2.9 ± 1.0 nm (Figure 1e and the inset of Figure 1f), of the three γ-Al_2O_3 samples. These data demonstrate that most of the Pt atoms in such a cluster will experience more bulklike bonding given the rather large number of atoms that it contains, $N_{avg} = 700$ (Figure 1f).

Analogous HAADF-STEM micrographs for two Pt/C nanocluster samples were recorded and size-distribution histograms analyzed (SI, Figure 10). Samples prepared using a protocol similar to that employed for the Pt/γ-Al_2O_3 samples yielded results comparable to the distribution of cluster sizes obtained (1.0 ± 0.3 nm). We also examined a commercial Etek, Inc. sample of Pt/C and found it to have an average diameter of 1.8 ± 0.5 nm (SI, Figure 7).

3.2. Electronic and Atomic Structural Characterization of Pt/γ-Al_2O_3. We start with a consideration of EXAFS results in two stages, both complementing the data reduction and analysis processes. First we examine the raw data to draw qualitative guidance regarding the nature of the demonstrated structural and dynamical behaviors. We then present raw quantitative data that has been analyzed in a manner that does not make any assumptions about the particles under consideration (e.g., particle shape). The discussion that follows organizes these analyses along three major headings that serve to highlight the interplay of the main factors that direct the temperature-dependent structural responses of supported Pt nanoparticles. These factors are: (a) cluster size, (b) effects of adsorbates, and (c) the chemistry-specific effects of the metal−support interactions. On the subject of metal−support interactions, it is important to recognize the role of sample preparation as it relates to the absence of low-Z scattering contributions (conventionally associated with particle−support bonding)[32,49−52] in the FT magnitudes of our samples. The lack of a Pt−O contribution to the radial distribution function has been observed in a previous study[53] in which a similar synthetic protocol was employed in the preparation of Pt/γ-Al_2O_3.

3.2.1. Structural Dynamics as Influenced by Cluster Size. The raw EXAFS data, in terms of $\chi(k)$ or the Fourier Transform amplitude, provide useful insights pertaining to the influences of particle size on the structural dynamics. It is difficult, in general, to discriminate uniquely between the effects of temperature and size based on the Fourier transform magnitude alone (Figure 2 for Pt/γ-Al_2O_3 and SI, Figure 11, for Pt/C). Consideration of the k-space data (Figure 2a,c), however, allows a quantifiable discrimination between these two factors. One notes, for example, that the EXAFS data collected for the three different sized Pt samples (Figure 2a), when measured at the same temperature, appear to scale uniformly in intensity throughout the entire k-region. This sensitivity to cluster size permits the extraction of quantitative information about particle sizes by varying the coordination numbers in the fits (Figure 2b), thus providing direct points of comparison to the results obtained using microscopy.[37] In the present case, the qualitative assessment described above suggests that the samples adopt self-similar atomic scale structures (i.e., that the variation of particle size within this range does not lead to exaggerated atomic reconstructions). The influences of temperature within a given sample, however, are quite different. For example, temperature-dependent EXAFS data for the 2.9-nm Pt/γ-Al_2O_3 sample is characterized by a monotonic increase of the disorder parameter (σ^2) with temperature. This is revealed as a dampening of the EXAFS oscillation intensity at higher k values (Figure 2c). Such trends denote the dominating effects of thermal disorder (Figure 2d),[37] and as we show below (and in Supporting Information (SI)), the quantitative aspects of the data are also very sensitive to the surface chemistry of the particles, such as might occur in either oxidizing or reducing atmospheres (SI, Figure 12).

We turn now to a more quantitative analysis of the EXAFS data. The quantitative results of the data analyses for all the samples are summarized in Tables 1−3. Using a previously described geometric model,[54,55] we find the values of the average first-nearest-neighbor (1NN) M−M coordination numbers for the three nanocluster samples are ones consistent with the average particle sizes obtained by TEM. Specifically, the extended atom counting analyses demonstrate the adoption of a more oblate shape of the particles with decreasing particle size (Figure 1b,d,f and SI, Figure 1). This strict validation of the analysis procedure supports a more detailed quantitative assessment where the assumption is made that the distribution of clusters in the sample can be represented by an "equivalent cluster", i.e. that the size distribution is narrow enough that EXAFS-based characterizations accurately exemplify properties that are intrinsic to a cluster of that size.[54,55]

Figure 3a provides a full comparison of the temperature dependences of the 1NN Pt−Pt bond lengths for all three Pt/

(48) Koningsberger, D. C.; Prins, R. *X-Ray Absorption: Principles, Applications, Techniques of EXAFS, SEXAFS and XANES*; John Wiley & Sons: New York, 1988.
(49) Oudenhuijzen, M. K.; Bitter, J. H.; Koningsberger, D. C. *J. Phys. Chem. B* **2001**, *105*, 4616.
(50) Reifsnyder, S. N.; Otten, M. M.; Sayers, D. E.; Lamb, H. H. *J. Phys. Chem. B* **1997**, *101*, 4972–4977.
(51) Oudenhuijzen, M. K.; van Bokhoben, J. A.; Miller, J. T.; Ramaker, D. E.; Koningsberger, D. C. *J. Am. Chem. Soc.* **2005**, *127*, 1530–1540.
(52) Vaarkamp, M.; Miller, J. T.; Modica, F. S.; Koningsberger, D. C. *J. Catal.* **1996**, *163*, 294–305.
(53) Munoz-Paez, A.; Koningsberger, D. C. *J. Phys. Chem.* **1995**, *99*, 4193.
(54) Frenkel, A. I.; Nemzer, S.; Pister, I.; Soussan, L; Harris, T.; Sun, Y.; Rafailovich, M. H. *J. Chem. Phys.* **2005**, *123*, 184701-1–/184701-6.
(55) Calvin, S.; Miller, M. M.; Goswami, R.; Cheng, S.-F.; Mulvaney, S. P.; Whitman, L. J.; Harris, V. G. *J. Appl. Phys.* **2003**, *94* (1), 778–783.

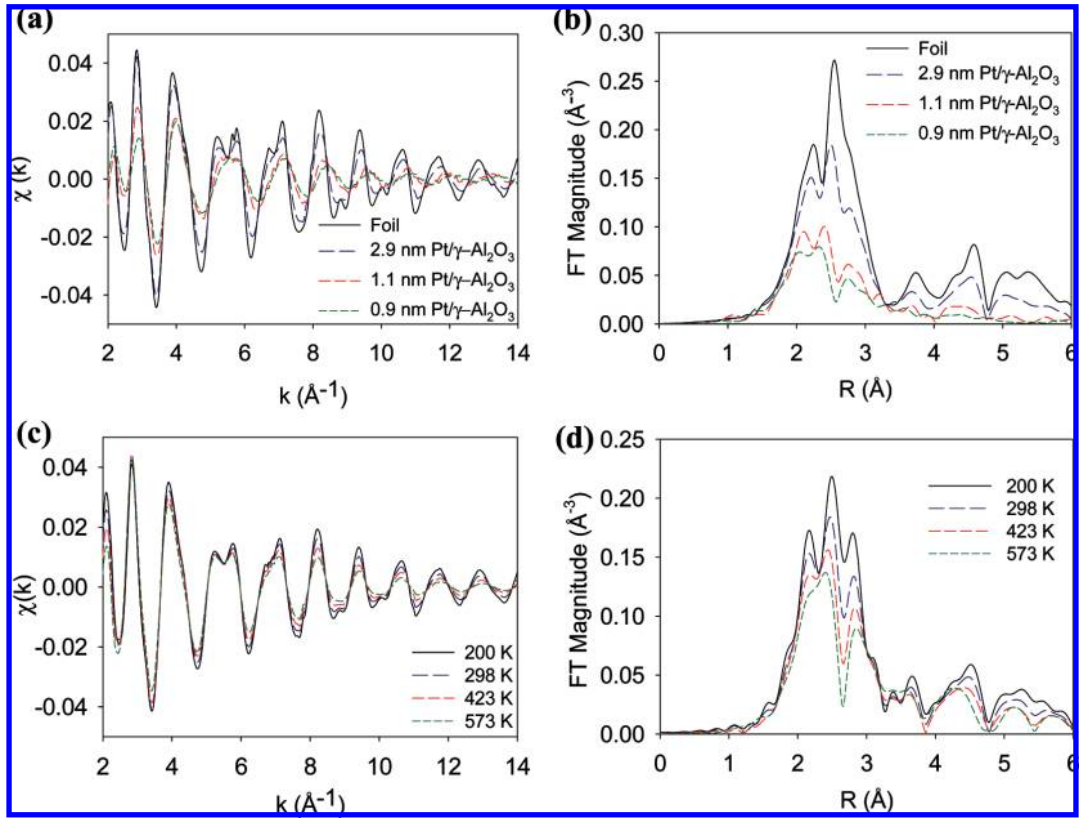

Figure 2. (a) EXAFS data in *k*-space illustrating the effect of cluster size on the oscillatory pattern of different Pt/γ-Al_2O_3 samples and a bulk foil standard (*k*-weight = 0, *k*-range = 2−14 Å^{-1}) with corresponding (b) Fourier transform magnitudes. (c) Progressive changes in intensity of the EXAFS data in *k*-space for a 2.9-nm Pt/γ-Al_2O_3 sample (*k*-weight = 0, *k*-range = 2−14 Å^{-1}) in response to temperature variation and (d) corresponding Fourier transform magnitudes with gradual changes in real space.

Table 1. Pt−Pt Coordination Numbers and Thermal Parameters of Pt/γ-Al_2O_3 Nanoclusters

	He							4% H_2 (balanced by He)						
sample	N_{Pt-Pt}	σ^2_{static} (Å^2)	θ_E (K)	average α 10^{-6} (K^{-1})	R_{RT} (Å)	ΔE_0 (eV)	reduced χ^2	N_{Pt-Pt}	σ^2_{static} (Å^2)	θ_E (K)	average α 10^{-6} (K^{-1})	R_{RT} (Å)	ΔE_0 (eV)	reduced χ^2
0.9 nm	5.5(2)	0.0069(3)	300(20)	−24(4)	2.686(8)	5.4(5)	14.6	5.9(2)	0.0052(2)	207(6)	−13(3)	2.739(7)	7.5(5)	8.9
1.1 nm	6.3(3)	0.0045(2)	226(7)	−14(5)	2.704(6)	6.4(4)	7.5	6.8(2)	0.0037(2)	204(5)	−15(2)	2.736(5)	7.0(3)	12.0
2.9 nm	9.7(1)	0.0021(1)	203(2)	2(1)	2.747(2)	7.9(2)	7.5	9.8(1)	0.0015(8)	200(2)	−6.0(2)	2.760(2)	7.9(2)	14.1
foil	12.1(2)	0.00017(8)	179(2)	11(1)	2.747(2)	8.6(3)	15.3							

Table 2. Fit Results and Thermal Parameters of Pt/C Nanoclusters

sample	N_{Pt-Pt}	σ^2_{static} (Å^2)	θ_E (K)	average α 10^{-6} (K^{-1})	R_{RT} (Å)	N_{Pt-C}	R_{Pt-C} (Å)	σ^2_{Pt-C} (Å^2)[a]	ΔE_0 (eV)	reduced χ^2_{Pt-Pt}	reduced χ^2_{Pt-C}
Under He											
1.0 nm Pt/C	5.4(2)	0.0029(2)	193(4)	2(4)	2.735(7)	0.9(2)	2.16(3)	0.000(4)	7.4(8)	3.0	324.4
1.8 nm Pt/C	7.7(1)	0.0023(1)	195(3)	10(2)	2.755(4)	0.7(2)	2.17(4)	0.000(6)	7.6(4)	5.3	633.4
Under H_2											
1.0 nm Pt/C	5.6(2)	0.0024(2)	189(4)	1(3)	2.747(7)	0.9(2)	2.13(4)	0.000(5)	7.7(8)	5.3	681.4
1.8 nm Pt/C	7.6(2)	0.0023(1)	196(3)	10(2)	2.755(3)	0.7(2)	2.17(4)	0.000(6)	7.8(5)	9.4	633.1

[a] Values at 293 K. Uncertainties exceed best-fit values.

γ-Al_2O_3 samples measured under He, along with data for a Pt foil used as a reference. The Pt foil exhibits the expected positive thermal bond length expansion with an average linear thermal expansion coefficient $\alpha = (1.1 \pm 0.1) \times 10^{-5}$ K^{-1}, an experimental value that agrees well with one derived from X-ray diffraction measurements ($\sim 0.88 \times 10^{-5}$ K^{-1} at 298 K).[56] The thermal behavior of the smallest 0.9-nm Pt/γ-Al_2O_3 sample provides marked contrasts with the bulk behaviors when measured under an inert He atmosphere. These clusters show two strong effects: first, a substantial relaxation of the static Pt−Pt pair distance compared to the bulk (by ~3%, denoted by R_{RT}, the Pt−Pt pair distances at room temperature in Table 1) and, second, a decrease of the pair distance with increasing temperature, with the former having been observed for many

(56) Touloukian, Y. S. *Thermophysical Properties of Matter*; Plenum Press: New York, 1975; Vol. 12.

Table 3. Fit Results and Thermal Parameters of Oxidized Pt/γ-Al_2O_3 Nanoclusters

	O_2										
sample	N_{Pt-Pt}	σ^2_{static} (Å^2)	θ_E (K)	average α 10^{-6} (K^{-1})	R_{RT} (Å)	N_{Pt-O}	R_{Pt-O}(Å)	σ^2_{Pt-O} (Å^2)[a]	ΔE_0 (eV)	reduced χ^2_{Pt-Pt}	reduced χ^2_{Pt-O}
0.9 nm	4.7(2)	0.0082(4)	350(43)	−29(4)	2.67(1)	0.8(2)	1.99(2)	0.006(3)	4.5(9)	3.7	74.1
1.1 nm	5.8(3)	0.0040(3)	199(7)	−14(7)	2.689(8)	0.6(2)	2.01(4)	0.008(5)	6.1(5)	10.9	43.1
2.9 nm	8.2(2)	0.0020(1)	192(4)	1(3)	2.747(8)	1.0(1)	1.99(1)	0.004(2)	8.9(6)	18.5	44.0

[a] Value at 293 K.

types of nanoparticle-support systems.[32−34,37,52,57−63] The average measured NTE coefficient α is $(-2.4 \pm 0.4) \times 10^{-5}$ K^{-1}. The data also revealed a nonbulklike thermal behavior for the 1.1-nm Pt/γ-Al_2O_3 nanoclusters qualitatively similar to, but less dramatic than, that of the smaller 0.9-nm clusters. In this case the measured α was $(-1.4 \pm 0.5) \times 10^{-5}$ K^{-1}. The data for the 2.9-nm Pt/γ-Al_2O_3 particles suggest a transition point to more bulklike properties as marked by an apparent positive expansion coefficient, $\alpha = (0.2 \pm 0.1) \times 10^{-5}$ K^{-1} (Table 1).

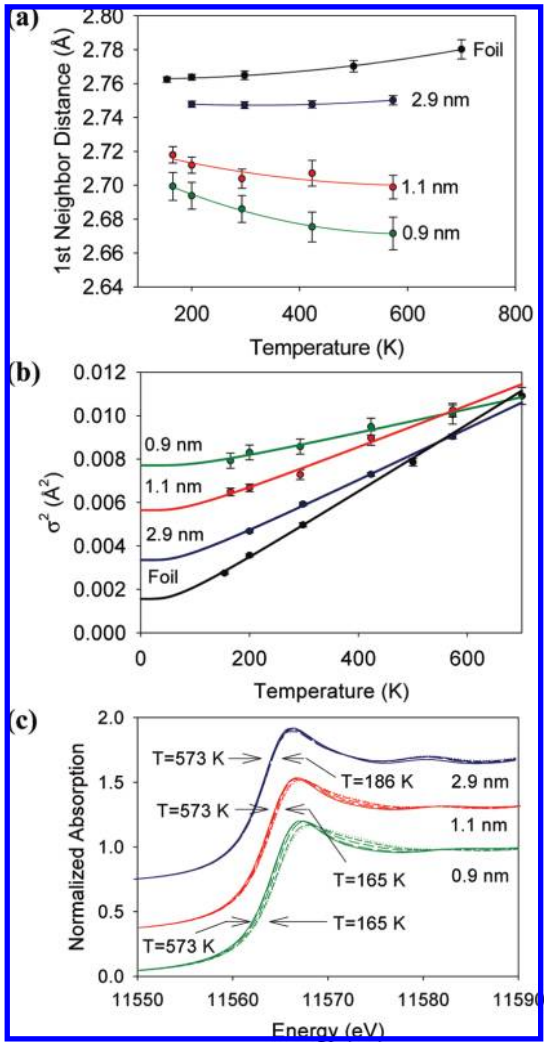

Figure 3. The role of nanoparticle size on structural dynamics is shown for the 0.9, 1.1, and 2.9-nm Pt/γ-Al_2O_3 samples. (a) Thermal dependence of the 1NN Pt−Pt bond distances for the different sized Pt/γ-Al_2O_3 nanoparticles compared to a Pt foil standard illustrating the effect of particle size on NTE. Note: the curves (solid lines) were inserted as aids to guide the eye. (b) Temperature dependence of the Debye−Waller factors (symbols), σ^2, for the various sized Pt/γ-Al_2O_3 nanoparticles and Pt foil plotted with their respective Einstein models (lines). (c) XANES behavior of the Pt/γ-Al_2O_3 nanoparticles for a given temperature range showing increasing sensitivity to temperature with decreasing nanoparticle size.

The functional dependences of the EXAFS Debye−Waller factors (σ^2) on temperature are also informative. These results are presented in Figure 3b. The data points correspond to the σ^2 values determined independently for each sample (under He) at a specific temperature while the lines are the corresponding fits made using a correlated Einstein model. The Pt foil data displays a very small contribution from static disorder, σ_s^2 (a measure of the temperature-independent, configurational disorder present in the sample), since its $\sigma^2(T)$ curve extrapolates to a value just slightly above zero, 0.0017 ± 0.0008 Å^2 at $T = 0$. This displacement from zero (the value expected for a perfectly ordered structure) is within the accuracy expected in such calculations. The calculated Θ_E (179 ± 2 K) is in excellent agreement with literature values (~180 K).[56] The 2.9-nm Pt/γ-Al_2O_3 nanoclusters exhibit a larger σ_s^2 (0.0021 ± 0.0001 Å^2) and also a higher Θ_E (203 ± 2 K). The 1.1-nm Pt clusters exhibit further increases in both the σ_s^2 (0.0045 ± 0.0002 Å^2) and Θ_E (226 ± 7 K). The data for the 0.9-nm clusters exhibit the largest perturbations, with σ_s^2 increasing to 0.0069 ± 0.0003 Å^2 and an apparent Θ_E of 298 ± 24 K.

Thermal perturbations of electronic structure are also evidenced in the larger sized samples. In the absence of specific temperature-dependent electronic effects, (e.g., metal−insulator transition) the XANES data should have little, if any, temperature dependence in terms of absorption edge position and shape, or white line intensity.[64] Such insensitivity has been demonstrated previously for Pt foil samples.[37] We found that the 2.9-nm diameter Pt/γ-Al_2O_3 sample yielded XANES data with a thermal dependence (Figure 3c) that is qualitatively similar to that of Pt foil.[37] In contrast, we observed substantial temperature-dependent changes in the XANES region of spectra measured in a He atmosphere for the 1.1-nm (Figure 3c), and even more dramatic ones for the 0.9-nm (Figure 3c), Pt/γ-Al_2O_3 nanocluster samples. In each case, the anomalous behavior was manifested as a progressive red-shift of the edge position and slight increase in the white line intensity with increasing temperature. We defer further comment on these points to the Discussion section.

3.2.2. Structural Dynamics as Influenced by Adsorbates. Experiments were carried out to explore the influences that adsorbates exert over the structural and dynamical responses of supported Pt catalysts. For the particle sizes considered here,

(57) Vaarkamp, M.; Mojet, B. L.; Kappers, H. J.; Miller, J. T.; Koningsberger, D. C. *J. Phys. Chem.* **1995**, *99* (43), 16067–16075.
(58) Moraweck, B.; Clugnet, G.; Renouprez, A. J. *Surf. Sci.* **1979**, *81* (2), L631–L634.
(59) Comaschi, T.; Balerna, A.; Mobilio, S. *Phys. Rev. B* **2008**, *77*, 075432-1−/01532-10.
(60) Kluth, P.; Johannessen, B.; Foran, G. J.; Cookson, D. J.; Kluth, S. M.; Ridgway, M. C. *Phys. Rev. B* **2006**, *74*, 014202.
(61) Kampers, F. W.; Koningsberger, D. C. *Faraday Discuss. Chem. Soc.* **1990**, *89*, 137–141.
(62) Sinfelt, J. H.; Via, G. H.; Lytle, F. W. *J. Chem. Phys.* **1982**, *76* (6), 2779–2789.
(63) Bus, E.; Miller, J. T.; Kropf, A. J.; Prins, R.; van Bokhoven, J. A. *Phys. Chem. Chem. Phys.* **2006**, *8*, 3248.
(64) Sinfelt, J. H.; Meitzner, G. D. *Acc. Chem. Res.* **1993**, *26*, 1–6.

such effects are expected to be significant given the considerable fraction of atoms residing at (or near) surface sites (particularly for the 0.9- and 1.1-nm clusters).[65−67] In the present study, this examination is particularly critical as the current literature does not present a clear picture regarding such interactions nor the mediating role they may play in modifying details of the interatomic bonding in very small clusters. For this reason, and to compliment the XAS measurements made under an inert He atmosphere (where the cluster present is presumably adsorbate free), we performed a similar set of measurements for samples maintained in a background pressure of hydrogen gas or after oxidation of the clusters in a dilute mixture of O_2 in He.

The impact of oxidation on the EXAFS spectra collected at room temperature for the three Pt/γ-Al_2O_3 samples is compared with that of their reduced counterparts in SI, Figure 12. Oxidation leads to marked decrease in the peak magnitude of the Fourier transform plots in the 2−3 Å range of the EXAFS data, which indicates a decrease in Pt−Pt coordination number and/or an increase of atomic disorder in the cluster. The scattering contribution seen between ∼1.5−2 Å is due to the Pt−O 1NN single scattering paths.

The influences of the H_2 atmosphere on the data are less dramatic. To provide a more quantitative analysis of the data, we consider in order the results of the temperature-dependent behaviors of the Pt−Pt bonds in three distinct chemical states as depicted in Figure 4: (1) oxidized clusters (O_2, in green) measured in helium; (2) reduced clusters after hydrogen desorption measured in helium (He, in blue); and (3) reduced clusters measured under a hydrogen atmosphere (H_2, in red). These data provide a basis to compare the associated structural dynamics for two types of adsorbates, O and H (Figure 4a). Of the three cluster sizes studied, the 0.9-nm Pt nanoclusters were impacted the most dramatically by the oxidative treatment (Table 3). Most important is the fact that the oxidative treatment induces a pronounced static contraction in the 1NN Pt−Pt bonds relative to either He or H_2 samples at all temperatures (Figure 4a). These clusters also exhibit NTE, but the value of α for the oxidized case is larger ($(-2.9 \pm 0.4) \times 10^{-5}$ K^{-1}, Tables 1 and 3). A lesser oxidation-induced bond contraction was observed for the 1.1-nm Pt nanoclusters, and there was no observable effect of oxidation in the 1NN Pt−Pt bond lengths found for the largest 2.9-nm Pt/γ-Al_2O_3 nanoclusters compared to the Pt foil (as reflected by the R_{RT} values found in Table 3). The influence of temperature on the bond lengths also diminishes with increasing cluster size (Tables 1,3).

Figure 4b in conjunction with Tables 1 and 3 presents data that demonstrate that the σ_s^2 term and the values of Θ_E (calculated for each Pt/γ-Al_2O_3 system) are well correlated across all cluster sizes for each of the various (He, H_2, and O_2) treatments. For all of the nanoparticle samples, the presence of H_2 in the ambient atmosphere results in a decrease of σ_s^2 for the Pt−Pt atom pairs (Table 1), consistent with the lifting of a surface relaxation due to hydrogen adsorption and resultant bulklike dynamics of the Pt atoms. For example, the 0.9-nm clusters under H_2 exhibit σ_s^2 of 0.0052 ± 0.0002 Å^2 and Θ_E of 207 ± 6 K. In the inert environment (He), the σ_s^2 increases to 0.0069 ± 0.0003 Å^2, with an apparent Θ_E of 298 ± 24 K. For

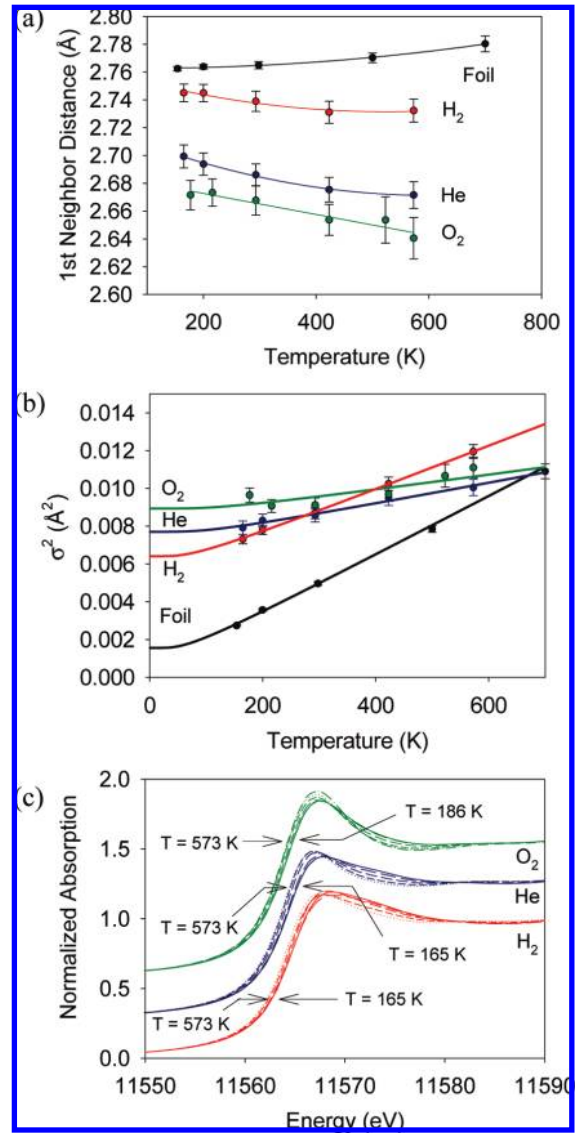

Figure 4. Observed adsorbate effect is shown for samples exposed to reactive (H_2, O_2) and inert (He) gas phase environments. (a) Result of particle−adsorbate interactions for the 0.9-nm Pt/γ-Al_2O_3 sample examined by measuring the temperature dependence of the 1NN Pt−Pt interatomic distances. (b) Dependence of the σ^2 (symbols) on temperature for a 0.9-nm Pt/γ-Al_2O_3 and Pt foil with the Einstein models (lines) included for the different ambient conditions studied. (c) Fluctuations in the XANES spectra of the 0.9-nm Pt/γ-Al_2O_3 sample for a series of temperatures as influenced by the absence/presence of adsorbate.

purposes of comparison, we also present the 1NN Pt−Pt σ^2 values for the oxidized samples in Figure 4b. The σ_s^2 and Θ_E determined from the correlated Einstein models for this sample are given in Table 3. The characteristics of σ^2 for the 0.9-nm Pt/γ-Al_2O_3 nanoclusters are markedly different from those of the H_2 and He cases. First, oxidation results in a statistically significant increase in the σ_s^2 in the Pt−Pt bonds in the nanoclusters. Second, there is an apparent increase in Θ_E. Notably, the correlated Einstein model does not appear to suitably correlate with the σ^2 determined independently at each measurement temperature. This is inferred by the large uncertainty that attends the calculation of the Θ_E (Table 3) within the Einstein model used in the data analysis.

The effects of adsorbates on the electronic structures of the clusters, as revealed by the changes appearing in XANES data, are illustrated by the spectra presented in Figure 4c. As expected,

(65) Lopez, N.; Janssens, T. V. W.; Clausen, B. S.; Xu, Y.; Mavrikakis, M.; Bligaard, T.; Norskov, J. K. *J. Catal.* **2004**, *223*, 232–235.
(66) Slovokhotov, Y. L.; Zubavichus, Y. V.; Beliakova, O. A. *Nucl. Instrum. Methods Phys. Res., Sect. A* **2000**, *448*, 302–307.
(67) Tomanek, D.; Mukherjee, S.; Bennemann, K. H. *Phys. Rev. B* **1983**, *28* (2), 665–673.

the impacts evidenced in the oxidized samples are qualitatively different from those found in either H_2 or He atmospheres (Figure 4c). The main difference between measurements made in each case is the correlated increase of the white line intensity. The dramatic nature of this electronic perturbation is further demonstrated by the marked blue shift of the isosbestic point seen with the increasing oxidation state of the Pt atoms in the cluster.

Systematic measurements of the size-, substrate-, and adsorbate-dependent thermal properties of the Pt clusters allow discrimination between the charge transfer effects of the substrate and adsorbates (O vs H) on the apparent contraction of the Pt−Pt bond lengths. The smallest γ-Al_2O_3 supported clusters exhibit NTE regardless of the atmosphere. The 2.9-nm clusters, however, illustrate a crossover region where these two effects (support and adsorbate interactions) can be quantitatively separated: the Pt−Pt bond length in these clusters expands positively under He atmosphere and negatively under H_2 (Table 1). The origin of the latter behavior is rooted in the temperature-dependent hydrogen coverage which decreases with increasing temperature.[49,52,63,68] Due to the cluster−support and cluster−adsorbate interactions, the ensemble-average from the EXAFS signal affords a weighted average of the electronic contributions of surface Pt atoms over the Pt atoms at the cluster−support interface. The proportion of each contribution is directly related to the relative fraction of surface atoms to interface atoms. Thus, it is plausible to find a combination of particle size and hydrogen coverage such that the particle demonstrates a bulklike response (conventional thermal expansion) under inert conditions while exhibiting NTE under H_2. We independently verified this prediction in control experiments that examined thermal behaviors of Pt/γ-Al_2O_3 clusters of a similar size but at a higher background pressure (1 atm) of H_2. These control experiments (SI, Figure 12) confirmed that the higher pressure provides a near-saturation coverage of hydrogen to temperatures as high as 573 K and a more bulklike response of the average Pt−Pt bond lengths. These data therefore define a size-dependent scaling of the electronic contributions of the metal−support interface within the ensemble average properties of a supported cluster.

3.2.3. Structural Dynamics as Influenced by the Support. The FT magnitudes of the EXAFS data for two Pt/C nanocluster samples measured under He at room temperature are given in the Supporting Information (Figure 11) along with data taken for a Pt foil standard. Of note in these data is the presence of a low-Z scattering contribution at $R < 2.0$ Å that is not observed in the data for the Pt/γ-Al_2O_3 systems under similar conditions (SI, Figures 5−7). This contribution was fit to a Pt−C scattering interaction involving the support (Table 2).

The temperature independent 1NN Pt−Pt coordination numbers for the carbon supported samples are presented in Table 2. These values are consistent with the microscopy-determined size distributions and favor a faceted hemispherical structure (SI, Figure 1).

The temperature-dependences of the bond lengths of the Pt/C nanoclusters, as measured under an inert He atmosphere, are presented in Figure 5a. It is immediately apparent that the 1.0-nm Pt/C sample does not exhibit NTE. Its thermal expansion coefficient ($(0.2 \pm 0.4) \times 10^{-5}$ K^{-1}) stands in contrast to the behavior of the 0.9-nm Pt/γ-Al_2O_3 sample described above. The

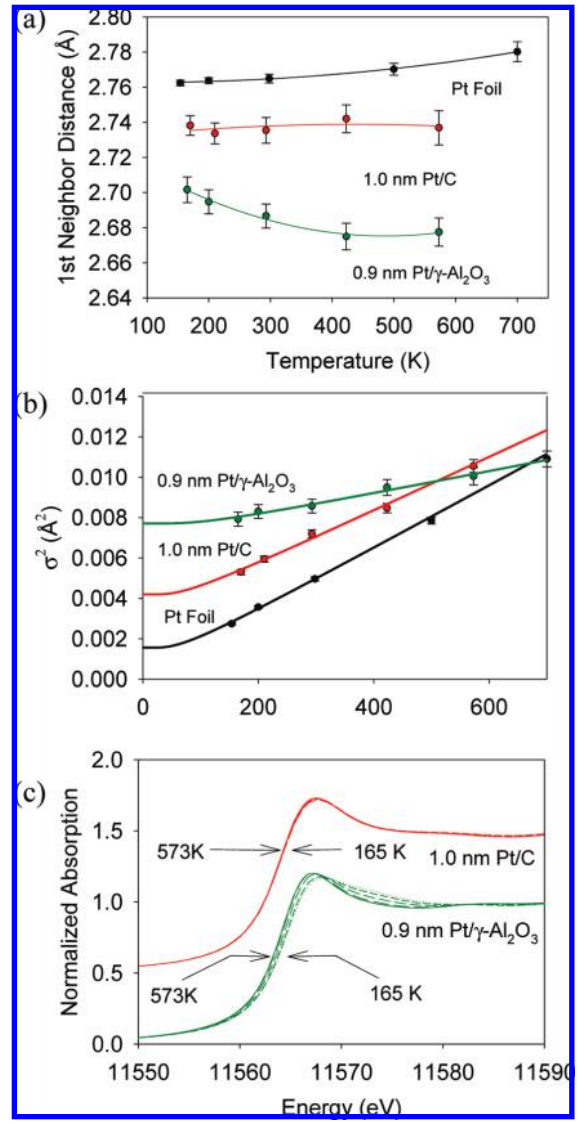

Figure 5. Effects of the support examined in terms of (a) temperature dependence of the 1NN Pt−Pt distances for 0.9-nm Pt/γ-Al_2O_3 and 1.0-nm Pt/C samples compared simultaneously with a Pt foil standard. (b) Contrasting behaviors of σ^2 with respect to temperature for the γ-Al_2O_3/C supported Pt particles and Pt foil plotted with their respective Einstein models (lines). (c) Monitored changes to XANES spectra for the 0.9-nm Pt/γ-Al_2O_3 and 1.0-nm Pt/C samples over a temperature range of 165 − 573 K and 170 − 573 K, respectively.

Pt/C nanoclusters do show size-dependent bond length relaxations compared to the bulk however (Figure 5a; see also R_{RT} values in Tables 1 and 2). The 1.8-nm Pt/C nanoclusters under He exhibit bond length relaxations of ∼0.4% from the bulk value. The presence of H_2 has little influence on the temperature dependence of the Pt−Pt bond lengths as indicated by an $\alpha = (1.0 \pm 0.2) \times 10^{-5}$ K^{-1} under both H_2 and He, a value quantitatively similar to that for bulk metal (Table 2). The bond lengths measured for the smaller 1.0-nm Pt/C nanoclusters under He are more significantly contracted by an apparent surface relaxation mechanism (∼1.1% relative to the bulk value). These data show that hydrogen adsorption increases the average bond lengths of the 1NN Pt atoms, consistent with the lifting of a surface relaxation by adsorbate (Table 2).

For Pt/C clusters, the best fit values of σ^2 for the Pt−C bonds were indistinguishable from zero, to within the uncertainties (0.004−0.006 Å^2, Table 2). Even though these parameters

(68) Ferreira-Aparicio, P.; Guerrero-Ruiz, A.; Rodriguez-Ramos, I. *Faraday Trans.* **1997**, *93*, 3563–3567.

cannot be accurately fit within the confines of the structural model, the larger inference remains that this bond is relatively stiff as compared to the Pt−O interaction in the Pt/γ-Al_2O_3 samples. The values of σ^2 for the Pt−Pt bond calculated from the data for the 1.0-nm Pt/C and 0.9-nm Pt/γ-Al_2O_3 samples are graphically presented in Figure 5b. The σ_s^2 and Θ_E for Pt/C as determined from the correlated Einstein models are provided in Table 2. The experimentally determined σ_s^2 value for the 1.0-nm Pt/C sample is larger than that of the bulk. Even so, this measure of bond-length disorder is substantially smaller than that found for the 0.9-nm Pt/γ-Al_2O_3. The magnitude of the σ_s^2 of the 1NN M−M bond lengths of the 1.0-nm Pt/C clusters is significantly reduced by H_2 adsorption, a behavior similar to that found for all of the Pt/γ-Al_2O_3 samples (Tables 1,3). There was no statistically significant dependence of Θ_E value calculated from the data that results from H_2 adsorption, a result that markedly differs from those for the γ-Al_2O_3-supported clusters. Finally, we note that the σ_s^2 values measured for the 1.8-nm Pt/C nanoclusters were not impacted by H_2 adsorption (Tables 1,2).

Figure 5c shows five XANES spectra, representing data collected under a He atmosphere at all measurement temperatures for the 1.0-nm Pt/C and 0.9-nm Pt/γ-Al_2O_3 samples (taken from Figures 3c and 4c) and plotted on the same scale to aid in their comparison. These spectra are qualitatively and quantitatively different. Most notably, there is a marked red shift and an increase in the normalized absorption intensity seen for the γ-Al_2O_3 supported sample. These thermally driven trends are not seen in the Pt/C system. Figure 3 shows these perturbations attenuate with increasing dimensions of the Pt/γ-Al_2O_3 clusters. The γ-Al_2O_3 support is therefore distinguished in this comparison by the significant electronic perturbations evidenced in the Pt clusters supported on it. The latter is a feature that is directly correlated with the occurrence of charge transfer, a topic addressed in the discussion section.

Taken together the data establish several points for comparison that are central to the size-dependent scaling of the structural dynamics of supported Pt nanoclusters. These trends are illustrated graphically in the plots given in Figure 6, where the metal cluster size is represented by the 1NN M−M coordination number determined by EXAFS (Tables 1,3). First, the particles exhibit significant contractions in their 1NN Pt−Pt bond distances relative to that of bulk metal, irrespective of the support (γ-Al_2O_3 or C). The magnitudes of these static bond length contractions correlate inversely with particle size. Second, small clusters (again irrespective of the support) also embed significant levels of disorder in their M−M bonding relative to bulk state, the magnitude of which is largest in the smallest clusters. Third, support interactions appear to contribute to electronic effects (in ways that are different for the Pt/γ-Al_2O_3 and Pt/C systems) that can strongly influence the structural dynamics of supported nanoscale clusters.

4. Discussion

The most significant finding coming from the measurements reported in this study is the unexpected complexity of the structural dynamics of supported metal nanoparticles, systems that well model important classes of industrial catalysts. Our results suggest marked structural sensitivities to three dominating factors: (a) particle size, (b) the chemistry of adsorbates, and (c) the nature of their interactions with the support. That the atomic structure of metallic clusters would be sensitive to such features is not a new idea. Such notions deeply inform long-

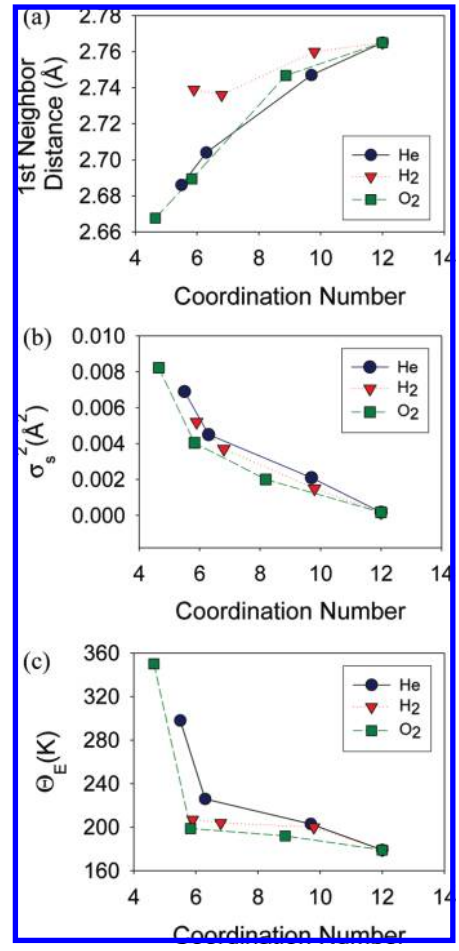

Figure 6. (a) Room temperature measurements of 1NN Pt−Pt bond distances, (b) the static component of the Debye−Waller factor, σ_s^2, and (c) the Einstein temperature, Θ_E, as a function of size for Pt samples (0.9-, 1.1-, and 2.9-nm Pt/γ-Al_2O_3 and Pt foil) measured in reduced (He and H_2) and oxidized states. Cluster size is denoted by coordination number, and the associated errors are tabulated (See Tables 1 and 3).

adopted, albeit qualitative, models of structure−property relationships in catalysis.[30,32−34,50,52,69] There remain, though, critical deficiencies in these models and a general lack of understanding of structure at the atomic level that complicates a formal method of explaining the associated dynamics. It is therefore useful to start with a consideration of model structures and bridge from these ideas to the more important concepts developed by the current work.

It is now well appreciated that qualitative models of metal clusters that idealize them as polyhedra with atoms occupying regular lattice positions are inadequate. From a structural standpoint, a number of studies have revealed increased strain in nanoparticles relative to the bulk metal, being manifested in such cases as significantly contracted bond distances and increased static structural disorder.[15,32−34,37,52,57−61,63,70−74] A

(69) Koningsberger, D. C.; Oudenhuijzen, M. K.; Bitter, J. H.; Ramaker, D. E. *Top. Catal.* **2000**, *10*, 167–177.
(70) Cleveland, C. L.; Landman, U.; Schaaff, T. G.; Shafigullin, M. N.; Stephens, P. W.; Whetten, R. L. *Phys. Rev. Lett.* **1997**, *79*, 1873–1876.
(71) Ankudinov, A. L.; Rehr, J. J.; Low, J. J.; Bare, S. R. *J. Chem. Phys.* **2002**, *116*, 1911–1919.
(72) Benfield, R. E.; Grandjean, D.; Kroell, M.; Pugin, R.; Sawitowski, T.; Schmid, G. *J. Phys. Chem. B* **2001**, *105*, 1961–1970.
(73) Zhang, P.; Sham, T. K. *Phys. Rev. Lett.* **2003**, *90*, 245502/1–245502/4.

variety of phenomenological models have been described in the literature that offer more atomistic detail such as those that include the relaxation of atoms in clusters due to surface effects,[75,76] reconstruction due to adsorbate-cluster interactions[34,50,61,69] and, most importantly, the basic principles involved in structural development that arise as a consequence of metal−support interactions.[30,32−34] Recent reports[77,78] applied new computational approaches toward the analysis of cluster−support interactions and the strong influences they exert on the structural dynamics of supported metal clusters. These studies, and the present work, demonstrate that the physical properties of prototypical supported metal clusters, at least within a narrow size range of 1−3 nm, can exhibit striking forms of complexity. The diversity of the effects established in this work−including: adsorbate-mediated atomic reconstruction of the cluster, significant examples of bond disorder, thermal mediation of electronic structure, and most notably, cluster size and support-dependent behaviors that lead to NTE−challenge current understandings of structural dynamics in nanoscale materials. Our studies specifically suggest that competing interactions are central in directing the mesoscopic behaviors found in Pt/γ-Al_2O_3 nanoparticles. In the sections that follow we develop these ideas and highlight quantitative and qualitative features associated with the chemical properties of this catalytic system.

Platinum is an indispensable catalyst, being among the most active metals known for the activation of H_2 for hydrogenation catalysis.[1−3] It also exhibits, along with a few other noble metals (e.g., Ir), the highest rates and selectivities in C−H and C−C bond activation and capacities for regeneration that lead to enhanced on-stream lifetimes.[2,3] For these reasons, Pt catalysts are essential for the efficient production of hydrocarbon fuels. Unfortunately, there remain significant deficiencies in current understandings of the atomistic details involved in the processes that this metal catalyst promotes.[37] This lack of basic understanding is only amplified by the complexities that attend its use in supported forms for processes involving chemically demanding environments.[30,32−34,50,52,61,69]

The present work examines fundamental dynamical behaviors in well-defined γ-Al_2O_3-supported Pt clusters in the size range of 0.9−2.9 nm. The acidic nature of this support promotes useful forms of C−C bond isomerization and, for this reason, finds ubiquitous use in hydrocarbon processing. The synergistic qualities of the γ-Al_2O_3 support and the Pt catalyst result in improved usage of the carbon content of feedstocks, resistance to deactivation by coking/sintering, improved processing lifetimes, and facility of regeneration.[2,3] The present work demonstrates interesting behaviors for Pt on this support, highlighting the catalyst's dependence on cluster size along with its sensitivity to the chemical influences of adsorbates and electronic perturbations to the cluster's M−M bonding that result from the cluster−support interactions. The latter serve to illustrate the requirements for more complex models to fully account for the bonding in such supported catalysts.[77,78]

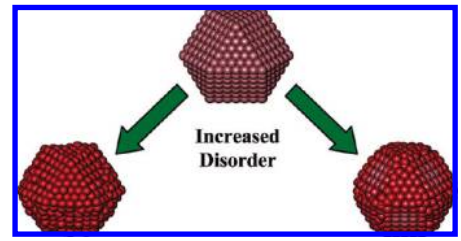

Figure 7. Top view of an idealized 2.9-nm Pt nanoparticle containing 500 atoms arranged with a truncated cuboctrahedral structure is shown in the center image. The structure on the left shows surface relaxation of the cluster atoms as computed using a molecular dynamics simulation. The structure on the right follows from a qualitative relaxation restricted to specific low coordination site atoms. In this latter cluster, atoms that are localized at their perfect lattice positions are shown in gray, and atoms in red indicate areas with increasing strain as compared to the idealized structure.

The most interesting result coming from the EXAFS measurements is the anomalous thermal behavior of the 1NN Pt−Pt bond distances seen in our supported nanoclusters (Figures 3a, 4a, and 5a). The occurrence of NTE for Pt/γ-Al_2O_3 nanoclusters is unexpected, given that the cluster bonding is expected to conform to a close-packed metal system. The most fundamental requirement for close-packed bonding, due to the anharmonicity of the interatomic potential, is that of thermal expansion in which the average M−M bond length increases with rising temperature. In rare cases, where bond bending can contribute, the vibrational motion can lead to a decrease in the volume of a solid material with temperature.[79] A classic example of such behavior is that of cubic zirconium tungstate, in which its open framework structure allows low-frequency transverse vibrational modes to contribute more strongly to the thermal properties of the crystal lattice than high-energy longitudinal modes, with the result being a net NTE.[79−82] Such forms of vibrational anisotropy cannot be supported within a close-packed metallic structure, however.[83] The qualitative models typically used to describe the bonding of supported clusters (e.g., a cuboctahedral structure) establish the M−M bonding in a way that is directly related to the FCC structure of bulk Pt. For this reason normal (i.e., more bulklike) thermal properties are to be expected.[37] Recent work has demonstrated, however, that size effects can complicate this picture. Bond relaxations (contractions in Pt−Pt bond distances), for example, provide prominent contributions to the structure of small clusters−a feature intuitively expected for systems heavily weighting the low-coordination environments of surface atoms within their net bonding.[13,67,75,76,84] More recent theory-based studies have demonstrated a striking capacity for anisotropy in such relaxations−that the bond relaxation need not occur uniformly in a single atomic layer at an interface but, instead, exhibit a broad variation among an array of sites on the cluster surface.[77,78] These ideas are depicted schematically in Figure 7, which presents molecular dynamics models that summarize in a qualitative fashion essential ideas related to the structures our data define for one of the Pt/γ-Al_2O_3 systems examined in this work. The scheme shows one model for a truncated

(74) Giovanetti, L. J.; Ramallo-Lopez, J. M.; Requejo, F. G.; Garcia-Gutierrez, D. I.; Jose-Yacaman, M.; Craievich, A. F. *J. Phys. Chem. C* **2007**, *111*, 7599–7604.
(75) Mays, C. W.; Vermaak, J. S.; Kuhlmann-Wilsdorf, D. *Surf. Sci.* **1968**, *12*, 134–140.
(76) Vermaak, J. S.; Mays, C. W.; Kuhlmann-Wilsdorf, D. *Surf. Sci.* **1968**, *12*, 128–133.
(77) Vila, F.; Rehr, J. J.; Kas, J.; Nuzzo, R. G.; Frenkel, A. I. *Phys. Rev. B* **2008**, *78*, 121404-1–/121404-4.
(78) Wang, L.-L.; Kare, S. V.; Chirita, V.; Johnson, D. D.; Rockett, A. A.; Frenkel, A. I.; Mack, N. H.; Nuzzo, R. G. *J. Am. Chem. Soc.* **2006**, *128* (1), 131–142.
(79) Barrera, G. D.; Bruno, J. A. O.; Barron, T. H. K.; Allan, N. L. *J. Phys. Condens. Matter* **2005**, *17*, R217−R252.
(80) Evans, J. S. O. *J. Chem. Soc., Dalton Trans.* **1999**, *19*, 3317–3326.
(81) Mary, T. A.; Evans, J. S. O.; Vogt, T.; Sleight, A. W. *Science* **1996**, *272*, 90–92.
(82) Sleight, A. W. *Annu. Rev. Mater. Sci.* **1998**, *28*, 29–43.
(83) White, G. K. *Contemp. Phys.* **1993**, *34* (4), 193–204.
(84) Belyakova, O. A.; Zubavichus, Y. V.; Neretin, I. S.; Golub, A. S.; Novikov, Y. N.; Mednikov, E. G.; Vargaftik, M. N.; Moiseev, I. I.; Slovokhotov, Y. L. *J. Alloys Cmpds.* **2004**, *382*, 46–53.

cuboctahedron shape, here depicting an orientation of the cluster with the cubic 111 axis perpendicular to the support. The model further assumes an energetic preference for terminating the cluster along low-index planes. The structure at center is a baseline unrelaxed model in which all atomic positions are placed at the average M−M bond distance found by EXAFS (2.747 ± 0.002 Å) at room temperature. The remaining two structures show two of several plausible versions for relaxing the M−M bond framework of this structure. The model on the left depicts a uniform contraction of all surface atoms. The structure on the right is one in which specific low M−M coordination environments (vertices, plane edges, etc.) are relaxed. The point of interest here is that EXAFS analysis does not allow us to discriminate between the two models of disorder. The difference between the models translates into different populations of Pt−Pt bond lengths which are all be characterized by values of σ_s^2 that we experimentally measure. More definitive answers can be obtained by first-principle calculations that take into account mesoscopic effects and can, therefore, be directly verified by EXAFS analysis.

It is not unexpected that adsorbates substantially modify the quantitative aspects of the static Pt−Pt bond relaxations (Figure 4b).[50,61,69] Under reducing conditions for example, the cluster surfaces dissociate H_2 and bind H atoms. These interactions soften the nondynamic bond contractions, relieving the strain due to relaxation of the surface Pt atoms. Under oxidizing conditions (O_2) the Pt−Pt bonds are more strongly contracted, exhibiting intense strain relative to bulk Pt−Pt distances of as much as 2.8% due to the electronic consequences of O adatoms terminating the cluster surface. Inert atmospheric conditions (He) afford Pt−Pt bond lengths lying between these two limiting cases. These general trends follow simple models for electronic structure in M−M bonding, namely changes to the d-state occupancy increasing/decreasing bonding character.[50,69] Charge transfer, due to adsorbates, leads to changes in the electron density of these states. This results in a heightened static contractive force in the case of O-adatoms (electron withdrawing) when compared to H-adatoms (electron donating). We note here that the data in Figure 4 demonstrate these features persuasively. Furthermore, Tables 1 and 3 illustrate the significant cluster-size dependencies of these contributions. These nondynamic contractions, ones due to surface-sensitive relaxations of the Pt−Pt bond distances,[32−34,37,52,57−63,75,76] are an aspect of structure that can be accounted for within a close-packed bonding model.

The EXAFS data presented above also demonstrate the size-dependent nature of the disorder that characterizes nanoparticle structure (Figure 3). As noted above, some aspects of nonhomogeneous distribution of static Pt−Pt bond contractions within the cluster can be attributed to low coordination sites, such as atoms at an edge or vertex, where atoms regress inward toward the particle (relaxation). It follows intuitively that the disorder must arise as a consequence of a population of bond-relaxations that broaden the width of bond length distributions. It was our interest in characterizing these latter influences that led us to originally examine the thermal dependence of the EXAFS data−a requirement to deconvolute static and dynamic contributions to the value of σ^2.[47] One also assumes that the heterogeneity that likely characterizes the cluster−support interactions could also accentuate the trends evidenced in the (size-dependent) degree of disorder present in the Pt−Pt interatomic bonding. The latter trends, though, are ones that can still be accommodated within a formal close-packed model of the cluster bonding. The origins of NTE in this system therefore must be more complex and involve factors other than vibrational anharmonicity. The nature of the electronic contributions that are likely involved is revealed by a systematic analysis of the NTE observed. First, the data show that it is a support-dependent phenomenon−of consequence for γ-Al_2O_3 supports and, from our data, essentially absent for carbon. Second, NTE scales with cluster size as the smallest clusters are those that are most significantly influenced by the energetics of the metal−support interactions. The transition range for the mesoscopic behavior of the Pt/γ-Al_2O_3 system is exceptionally narrow. One notes, for example, that the EXAFS data for the 2.9-nm clusters, while still showing appreciable Pt−Pt bond length contractions relative to the bulk, display a thermal dependence of the bond lengths that is similar to that measured for bulk Pt with one notable exception: measurements made under a H_2 atmosphere (which convolve a stronger contribution from the temperature dependence of the hydrogen coverage). The data obtained under He essentially deconvolutes this coverage-dependent effect from other contributions and reveals a more bulklike (i.e., positive thermal expansion) response of the Pt−Pt bond lengths for the 2.9-nm samples (Table 1). It is striking that the smaller particles exhibit NTE under all ambient conditions explored in this work. This demonstrates a crossover between perturbation sensitive and more bulklike thermal effects in the 1.1−2.9 nm size range. A similar crossover between nanoscale and bulklike responses was recently reported in a separate study of Au nanoclusters−an NTE attributed in this instance to electronic influences dominating over vibrational effects as particle size decreased.[59]

What then are the electronic origins of the NTE observed for the smallest particles? To answer this question, it is instructive to consider the temperature-dependent changes seen in the XANES spectra presented in Figure 5c. It is well established that XANES reports sensitively on perturbations of electronic structure that are common to nanoscale materials. For example, varying the acidity of the metal oxide support has been found to impact the edge position, white line intensity, and edge shape of Pt-XAS data due to polarization and charge transfer effects.[32,51,71,85,86] As noted above, dynamic features of the particle−support interactions must also play a critical role in the observed temperature-dependent XANES spectra.[77,78] Considering the 0.9-nm Pt/γ-Al_2O_3 sample as a specific example, the HAADF-STEM data show that a representative cluster contains only on the order of 10−15 atoms;[17] given the relatively low (experimental) 1NN coordination number of 5.5 (Table 1), one infers that essentially every atom in one of these particles resides at either the surface or support interface. The energetics, in this instance, must weight the contributions of such sites significantly.

We believe the XANES data demonstrate a flow of charge between the Pt nanoparticles and the γ-Al_2O_3 support. The data in Figures 3c, 4c, and 5c show that white line intensity increases at elevated temperatures, indicating a progressive depletion of the occupied electronic states at the Fermi level, while at lower temperatures a decrease and broadening is observed, features consistent with the occurrence of a temperature-mediated charge transfer.[32,51,71,85,86] Two possible origins for this behavior are (a) a charge transfer from the support to the particle that dissipates at high temperatures or (b) a charge transfer from

(85) Ankudinov, A. L.; Rehr, J. J.; Low, J. J.; Bare, S. R. *Top. Catal.* **2002**, *18*, 3–7.
(86) Mojet, B. L.; Ramaker, D. E.; Miller, J. T.; Koningsberger, D. C. *Catal. Lett.* **1999**, *62*, 15–20.

the particle to the support that progressively increases with temperature. The XANES data offer a model-independent basis for concluding that the underlying effect is one involving a decrease of charge on the nanoparticle at heightened temperatures as discussed below.

It is frequently noted in literature that the edge shift can be used to discriminate between mechanisms involving charge transfer either on to (negative, or red, shift) or from (positive, or blue, shift) an absorbing atom.[48,87] Such relationships do indeed exist for many bulk materials—most notably oxides, where the main contributor to the edge shift comes from changes in the core hole screening upon charge transfer (a final state effect).[48,87] In nanoscale metal clusters, changes in the Fermi level due to charge transfer can also give rise to a set of opposing trends: red shifts with a decline of electron density and blue shifts with its accumulation. Since the two effects (screening and Fermi level change) can exert opposing influences on the X-ray absorption edge position, the sign of the direction of an edge shift with temperature alone cannot be used to determine the path of charge transfer. Other considerations, then, must be brought to bear to account for the trends seen in the XANES data (Figures 3c, 4c and 5c). It is instructive to consult literature precedent for thermal effects of the form established in the present work.

In a leading study, nearly identical thermally driven changes in the XANES spectra (a red-shift, increase in white line intensity, and edge narrowing at increasing temperatures) were reported to occur for Pt/SiO_2 catalysts under both He and H_2 atmospheres by Lytle et al. (no information on the thermal influences on the Pt−Pt bond distances was provided, however).[88] They ascribed these changes to the progressive thermal breaking of bonds to surface oxygen atoms of the support, a hypothesis supported by the disappearance at high temperature of a Pt−O scattering contribution observed at the lowest measurement temperatures (90 K). An alternative explanation, and one supported by recent DFT/MD calculations, involves significantly increased disorder in the Pt−O bonding at higher temperatures that serves to essentially "wash out" the EXAFS from the Pt−O scattering pair,[77] subsequently modifying the interfacial structure associated with the transfer of charge. These are important consequences that support the idea of charge transfer from the support as an underlying mechanism.

Theoretical studies examined a model Pt_{10} cluster on the "d" layer of the [110] surface of γ-Al_2O_3.[77] This work successfully reproduced many of the puzzling behaviors documented in the present (and notable past) work, including NTE and corresponding XANES related electronic effects detailed above. This study emphasized the interrelatedness of these phenomena, providing new and general insights into the dynamics of supported metal nanoclusters. The simulations reveal dynamical consequences for bonding that derive from a differentiated structure, one comprising discrete layers of "oxidized" Pt atoms (those bonded to support oxygen atoms, designated Pt_O) and metallic-like Pt atoms (with solely Pt neighbors, designated Pt_M). These calculations showed that, as the temperature increased from 165 to 573 K (i.e., identical to the experimental temperature range described above), the average distances of the interlayer Pt_O-Pt_M bonds expanded markedly but were offset by larger contractions of the intralayer Pt_O-Pt_O and Pt_M-Pt_M bonds. These structural behaviors, as dictated by M-supported charge transfer, result within the theoretical model in a net and progressive NTE of the average Pt−Pt bond distances.[77,89] The most significant finding that emerges from this work, one that finds some support in the current literature, is that the structures adopted by nanoscale-supported metal clusters embed significant amounts of disorder.[15,37,70−74] The discussion above touches on one component of this disorder, the aspects that follow from the vibrational dynamics of specific M−M bonding pairs and their interactions with nonmetal-center bonding contacts involving either support or adsorbate atoms. This theoretical study suggested that additional dynamical components are involved and merit careful consideration; i.e. significant impacts on bonding can result as a direct consequence of highly fluxional, nonvibrational dynamics. The present work demonstrates explicit cases where supported metal clusters can exhibit large amplitude librational motions that strongly impact the cluster's atomic and electronic structures, aspects not previously considered in the context of supported metal catalyst particles. Future work is warranted to more completely examine the role of librational atomic motion in real catalytic systems, thereby establishing how they might modify site-specific forms of reactivity and/or stabilize clusters against sintering among other possibilities.

We now turn to a discussion of the surprisingly complex forms of bond disorder (as defined by σ_s^2) that can contribute to the ensemble structural properties of supported nanoclusters. The data presented above demonstrate that the Pt atoms in the nanoclusters exhibit disorder as nonvibrational deviations from their idealized atomic positions on periodic (e.g., fcc) sites—an embedded disorder. Such deviations have been noted by others and ascribed to a variety of effects including surface tension,[75,76] adsorbate induced strain,[50,54,61,74] as well as nonvibrational dynamics (such as the long period librational motions discussed above).[77,78] For all of the γ-Al_2O_3-supported clusters examined here, exposure to H_2 resulted in a significant decrease of σ_s^2 for 1NN Pt atom pairs, quantitatively correlating with a lifting of surface relaxation. Consistent with this model, the data show that the 0.9-nm clusters exhibit the largest response to hydrogen, presumably due to the higher fraction of metal atoms residing at surface sites. The anomalously high Θ_E (207 K under H_2 vs 298 K under He) in this case suggests that, while the correlated Einstein model can adequately fit the experimental data, the underlying assumption that vibrational degrees of freedom strictly embody cluster dynamics neglects important aspects of the physics involved. The latter conclusion is one that is strengthened by the nonbulklike anomalies noted in thermal expansion (the apparent NTE), XANES data (red shift), and large librational and static structural disorder revealed in DFT/MD and FEFF8 simulations.

The anomalous nature of σ^2 and the high values of Θ_E in such cases are difficult to reconcile within a simple model involving solely thermal populations of vibrational states of a single underlying equilibrium structure. If the latter were the case, the materials would be characterized by a temperature-independent anharmonic effective pair potential (a model often used in textbooks to visualize conventional thermal expansion). The temperature-dependent charge transfer, as strongly evidenced in the XANES data, implicitly establishes the importance of interactions that serve to continuously modify the total energy

(87) Sinfelt, J. H.; Meitzner, G. D. *Acc. Chem. Res.* **1993**, *26* (1), 1–4.
(88) Lytle, F. W.; Greegor, R. B.; Marques, E. C.; Sandstrom, D. R.; Via, G. H.; Sinfelt, J. H. *J. Catal.* **1985**, *95*, 546–557.
(89) Theoretical experiments, then, show a highly consistent picture, with the former establishing the essential underpinnings of dynamics in the mediation of thermal influences on the metal−support and Pt−Pt bonding.

of the supported clusters (doing so on γ-Al_2O_3 in ways that lead to NTE). As a result, the data require that the effective pair potential curve would need to be redefined at each temperature. Vila et al.,[77] confirmed this idea, revealing that the simulated nanocluster structure was in fact dynamic, with transient bonding and topology exhibiting stochastic motion of the center of mass on time scales long compared with internal vibrations. These librational motions lead to Pt−O bond breaking and formation very much in line with the prescient notion of Lytle et al.,[88] producing a level of disorder in the simulations that is consistent with the results found in experiment and the low amplitudes that preclude direct characterization of Pt−O bonding in the EXAFS. More importantly, their temperature-dependent, nonvibrational contribution to the bond disorder fully accommodates contributions that cannot be accounted for by the correlated Einstein model used to fit the experimentally determined σ^2 (eqs 1 and 2). One must instead substitute time- and configuration-dependent averaging to characterize static and dynamic contributions to the Debye−Waller factors.[37,47]

We now turn our attention to the effect of adsorbates (hydrogen and oxygen) on the electronic structure of Pt/γ-Al_2O_3 nanoclusters. The spectral changes shown in Figure 5c, and reported by others, include a red-shift of the absorption edge, decrease in white line intensity, and peak narrowing on the high-energy side at elevated temperatures. Such changes have been explained variously as being due to the creation of Pt−H antibonding states, Pt−H scattering, induced changes in Pt−Pt scattering, and changes in the atomic background scattering potential (i.e., the atomic X-ray absorption fine structure (AXAFS)).[51,90−93] The relative importance of these contributions remains controversial and a subject of much debate.[51,91,92] The present data demonstrate an important caveat, that such changes are not solely a characteristic of hydrogen on the Pt/γ-Al_2O_3 nanoclusters, given their absence in data for the Pt/C samples (Figure 5 and Table 2) that clearly show very similar relaxation effects of hydrogen viz. the Pt−Pt bond distances. Ultimately, the data convey the crucial role of the bonding occurring at the particle−support interface. These inferences are further reinforced by the oxygen data, which reflect conditions that cannot accommodate hydrogen bound at an ambient cluster interface. Important consequences for structure do attend the bonding of these adsorbates, however, as discussed below.

H_2 adsorption lifts the surface relaxation of the Pt−Pt bond distances. The sharing of electron density with antibonding states weakens the bonding character of the M−M bonds in the cluster.[50,69,90] It is not surprising, then, that H_2 adsorption also affects the magnitude of the NTE. This trend is particularly evident in the data for the 0.9-nm Pt/γ-Al_2O_3 nanoclusters, for which $\alpha = (-1.3 \pm 0.3) \times 10^{-5}$ K^{-1} under H_2 and $(-2.4 \pm 0.4) \times 10^{-5}$ K^{-1} under He (Table 1). We believe the overall weakening of the Pt−Pt bonds likely diminishes the dissimilarities between the differentiated forms of Pt−Pt bonding (Pt_M and Pt_O) revealed by recent DFT/MD calculations. With hydrogen acting as a weak electron donor, one expects it to diminish the σ_s^2 while increasing its temperature dependence via the weakening of the M−M bonding structure in the cluster. The effects are in fact observed experimentally with the latter manifesting more bulklike behavior and improved descriptive competency of the correlated Einstein model (Figure 4).

The impact of oxygen atom coordination on the nanoclusters has very different effects, notably inducing significant Pt−Pt bond contractions by withdrawing electron density from the cluster. The particle size dependence aspects of this data clearly reveal the significant consequence that oxygen bound at surface sites results in a stiffer M−M bonding network (Figure 4 and Table 3). The smallest (0.9 nm) Pt/γ-Al_2O_3 nanoclusters are impacted most dramatically by coordinated O adatoms. The Pt−Pt bond lengths in this case contract substantially, the observed NTE is larger in magnitude, and the σ_s^2 is the largest found in any of the experiments (Table 3). These oxidized subnanometer clusters exhibit structural and electronic properties that markedly differ from those of the bulk metal.

We close with a final consideration of broader trends revealed in the size-dependent emergence of mesoscopic behaviors in the Pt/γ-Al_2O_3 system and the consequences that such factors may hold with respect to their catalytic properties. The static contractions of the Pt−Pt bond lengths (due to surface relaxation) correlate strongly with cluster size and are neither unprecedented nor unexpected.[32−34,37,52,57−63,75,76] These bond strains, ones akin to surface relaxation in a bulk crystal, serve to compensate for the low average Pt−Pt coordination numbers.[13,67,75,76,84] The present work, however, demonstrates a somewhat more surprising trend, namely that the perturbations that come from atoms experiencing metal−support interactions can in fact rival, or possibly exceed, those due to M−M bonds involving atoms lying at the cluster's ambient interface (the latter region being where the influences of adsorbate must be most strongly weighted). The ensemble-average picture of atomic and electronic structure offered by XAS has served to mask the strong, and materials-dependent, influences of the metal−support interactions. Such bonding can be richly diverse even for samples composed of limited distributions of atomic mass. It remains, however, that specific dynamical sensitivities are expressed differently in the XAS data. The long-period, large-amplitude librations that MD/DFT suggests are critically important for Pt/γ-Al_2O_3, provide a notable case in point.[77] Vila et al.[77] show that the latter low-frequency motion of the cluster center of mass follows a form analogous to that of a two-dimensional Brownian-like motion (center of mass speed, $v = (2k_BT/m)^{1/2}$, where m is the cluster mass). This motion, given its explicit dependence on $1/\sqrt{m}$, will be much more significant for small clusters.

The present data, while extensive, leave a critical feature of the Pt/γ-Al_2O_3 systems unsatisfactorily defined−the atomistic architecture of the metal−support interactions that are central to the properties of this prototypical catalyst system. Part of the deficiency results directly from the considerable uncertainty regarding the atomic structure of the particle−support interface.[30−33,35,52] For example, any truncation of the supports bulk structure must present considerable chemical complexity−including strongly perturbing defects such as oxygen atom vacancies−at a terminating boundary. The XAS data tells us little of utility vis-à-vis the bonding arrangements that a supported Pt cluster adopts at these latter interfaces. The most likely inference to draw is that these interactions are both fluxional and subject to heterogeneity (supporting the presumption of significant disorder).[77] All the same, it remains likely that the substantial electronic perturbations are also the result of other contributing

(90) Ankudinov, A. L.; Rehr, J. J.; Low, J.; Bare, S. R. *Phys. Rev. Lett.* **2001**, *86*, 1642–1645.
(91) Ankudinov, A. L.; Rehr, J. J.; Low, J. J.; Bare, S. R. *Phys. Rev. Lett.* **2002**, *89*, 139702/1.
(92) Ramaker, D. E.; Koningsberger, D. C. *Phys. Rev. Lett.* **2002**, *89*, 139701/1.
(93) Ramaker, D. E.; Mojet, B. L.; Oostenbrink, M. T.; Miller, J. T.; Koningsberger, D. C. *Phys. Chem. Chem. Phys.* **1999**, *1*, 2293–2302.

factors which strongly weight the compositional morphology of the support. We believe strong cluster interactions with O atom vacancies on the support may critically contribute to the dynamic behavior of the supported cluster, an inference supported by theoretical study.[77] Future work will be needed to characterize such aspects more definitively, given the critical role that γ-Al_2O_3 appears to play as a support that improves the properties of Pt catalysts. Studies using atomic resolution STEM are currently in progress toward this end.

5. Conclusions

We describe the systematic analysis of the complex thermal behaviors of well-defined supported Pt catalysts by measuring their structural and electronic properties *in situ*. These temperature-dependent measurements revealed nonbulklike behavior (NTE, anomalous electronic properties, and large static disorder) in the smallest Pt/γ-Al_2O_3 nanocluster samples under O_2, He, and H_2 atmospheres. The coincidence of temperature-mediated changes to the electronic structure (observed by XANES) and atomic structure point to the inadequacy of cluster models described only by vibrational dynamics. Our results reveal that mesoscopic phenomena originate from the complex interactions occurring between the Pt clusters and the support under the mediating influences of adsorbates. Adsorption of hydrogen on the Pt/γ-Al_2O_3 nanoclusters reduces the cluster−support interaction by lifting contraction due to surface relaxation of the Pt−Pt bonds while oxidation of the particles increases the support-mediated impacts by increasing the strain and decreasing the electron density in the cluster. Similar measurements made on Pt nanoclusters supported on a carbon black reveal much weaker support effects than are seen for the γ-Al_2O_3-supported samples. Systematic interpretation of EXAFS and XANES measurements of such supported clusters offers an innovative methodology for elucidating support- and adsorbate-mediated changes to the electronic and atomic structures of the nanoparticles. Such insights into the structure and dynamics of nanoscale materials is required to enable the rational design of systems with desired properties, a goal particularly relevant to improving the performance of catalysts and other functional nanomaterials.

Acknowledgment. This work was sponsored in part by grants from the U.S. Department of Energy (DE-FG02-03ER15476). Experiments were carried out in part at the Frederick Seitz Materials Research Laboratory Central Facilities, University of Illinois, which are partially supported by the U.S. Department of Energy under Grants DE-FG02-07ER46453 and DE-FG02-07ER46471. Research was also carried out at the National Synchrotron Light Source (NSLS) at Brookhaven National Laboratory and at the Advanced Photon Source (APS) at Argonne National Laboratory. Use of the NSLS was supported by the U.S. Department of Energy, Office of Science, Office of Basic Energy Sciences, under Contract DE-AC02-98CH10886. Beamline X18B at the NSLS is supported in part by the Synchrotron Catalysis Consortium, U.S. Department of Energy Grant DE-FG02-05ER15688. The use of the APS was supported by the U.S. Department of Energy, Office of Science, Office of Basic Energy Sciences, under Contract No. DE-AC02-06CH11357. The authors acknowledge Paul Zschack and Jenia Karapetrova for their assistance in performing XAS experiments at the APS.

Supporting Information Available: Plots of EXAFS spectra, data with accompanying fits, associated EXAFS data analysis, and analytical electron microscopy data. This material is available free of charge via the Internet at http://pubs.acs.org.

JA809182V

SUPPORTING INFORMATION

The Emergence of Non-Bulk Properties in Supported Metal Clusters: Negative Thermal Expansion and Atomic Disorder in Pt Nanoclusters Supported on γ-Al_2O_3

Sergio I. Sanchez,[†] Laurent D. Menard,[†] Ariella Bram,[‡] Joo H. Kang,[†] Matthew W. Small,[†] Ralph G. Nuzzo,[*,†] and Anatoly I. Frenkel[*,‡]

Contribution from the School of Chemical Sciences and the Frederick Seitz Materials Research Laboratory, University of Illinois, Urbana, Illinois 61801 and the Department of Physics, Yeshiva University, New York, New York 10016

E-mail: r-nuzzo@uiuc.edu, anatoly.frenkel@yu.edu

Supporting Information.

S. I. Figure 1. Quantitative determination of geometric structure of the nanoparticles determined by the integrated areal intensity obtained from HAADF-STEM images. Representative particle diameters are plotted with respect to their integrated intensities (filled circles) for the (a) 0.9±0.2 (b) 1.1±0.3 and (c) 2.9±0.9 nm Pt/γ-Al_2O_3 . The curves represent guides correlated with integrated areal intensities for monolayer, cuboctahedral and truncated cuboctahedral nanoparticle structures. The average number of atoms found for the clusters in each sample is shown as N_{avg} with ± values representing the average of the calculated standard deviations.

S.I. Figure 2. Representative data showing the temperature reversibility of the 2.9 and 0.9 nm Pt/γ-Al_2O_3 samples as depicted by their k-space data (a and b), their subsequent Fourier transform (c and d) and the XANES data (e and f) (2.9 and 0.9 nm respectively). The temperatures experienced during the heating procedure were a high temperature of 573 K (573 K) and a low temperature of 185 K (165 K) for the O_2 (H_2) environment.

S.I. Figure 3. k-space data (a), the subsequent Fourier transform (b) and the XANES data (c) showing reversibility of cluster structure and electronic state are shown for the 2.9 nm Pt/γ-Al_2O_3 sample investigated. The temperature of the reduction and oxidation was 573 K.

S.I. Figure 4. Pt-Pt Coordination numbers as a function of temperature, for the smallest (0.9nm) and the largest (2.9nm) samples in He and H_2 on γ-Al_2O_3 support. The trend

shows very weak dependence on temperature (same effect was also observed in Pt foil when its coordination number was allowed to vary, which is, evidently, an artifact of the analysis) and thus can be ignored by fixing the coordination number to be constant in the fit.

S.I. Figure 5. Data for 2.9-nm Pt/γ-Al_2O_3 sample plotted with best fits in reduced states under inert (He) and reducing (H_2) atmospheres analyzed for a series of temperatures.

S.I. Figure 6. Data for 1.1-nm Pt/γ-Al_2O_3 sample plotted with best fits in reduced states under inert (He) and reducing (H_2) atmospheres analyzed for a series of temperatures.

S. I. Figure 7. Data for 0.9-nm Pt/γ-Al_2O_3 sample plotted with best fits in reduced its reduced state under inert (He) and reducing (H_2) atmospheres analyzed for a series of temperatures.

S. I. Figure 8. Examples of the difference file technique used to isolate and fit the low-Z contributors shown here for the low (186 K) and high (573 K) temperature measurements made for the oxidized (O_2) 2.9 nm Pt/γ-Al_2O_3 samples. (a) and (c) show the Fourier transform magnitudes of the raw data and fitting of the Pt-Pt first-nearest-neighbor (~2.1-3 Å) at 186 and 573 K, respectively. Subtraction of the theoretical fit from the experimental data and fitting (~1.4-2 Å) of the remaining low-Z scattering contributions at 186 and 573 K, shown for (b) and (d) respectively.

S. I. Figure 9. Examples of the difference file technique used to isolate and fit the low-Z contributors shown here for the low (170 K) and high (573 K) temperature measurements made for the 1.8 nm Pt/C samples under He flow. (a) and (b) show the Fourier transform magnitudes of the raw data plotted with the corresponding fits for the Pt-Pt first-nearest-neighbor (~2.1-3 Å) at 170 and 573 K, respectively. Subtraction of the theoretical fit from the experimental data and fitting of the remaining low-Z scattering contributions (~1.4-2 Å) at 170 and 573 K shown for (c) and (f), respectively.

S. I. Figure 10. HAADF-STEM images of (a) 1.0-nm and (b) 1.8-nm Pt nanoparticles supported on carbon black with the associated size distribution histograms (c) and (d).

S. I. Figure 11. Room temperature Fourier transform magnitudes for the 1.0 and 1.8 nm Pt/C samples plotted with the Pt foil standard.

S. I. Figure 12. Comparison of the Fourier transform magnitudes (k^2, k=2-13 $Å^{-1}$) of Pt/γ-Al_2O_3 samples in their oxidized and reduced states. The spectra shown were collected at room temperature for reduced (H_2) or oxidized (O_2) nanoclusters. (a) 2.9-nm Pt/γ-Al_2O_3, (b) 1.1-nm Pt/γ-Al_2O_3, and (c) 0.9-nm Pt/γ-Al_2O_3 nanocluster samples.

S. I. Figure 13. Control experiment showing behavior of the 1st neighbor distance of the Pt-Pt bonds under 5% H_2 gas mixture (balance He) and ultra-high purity hydrogen gas for the 2.9 nm Pt/γ-Al_2O_3 sample. Both data sets plotted simultaneously with Pt foil data.

S. I. Table 1. Tabulated values of the $\sigma^{(3)}$ values determined by fitting of the experimental data for each temperature-atmosphere combination and separated by particle size.

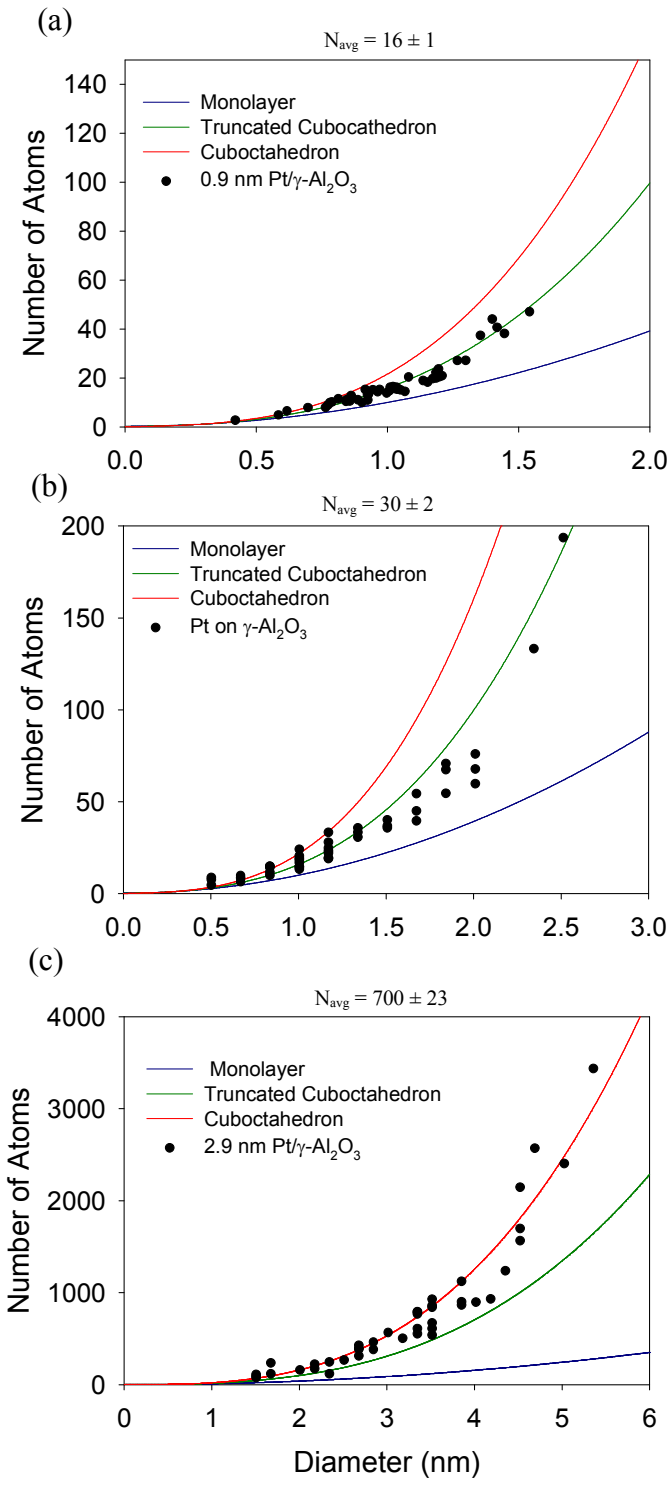

Supporting Information Figure 1.

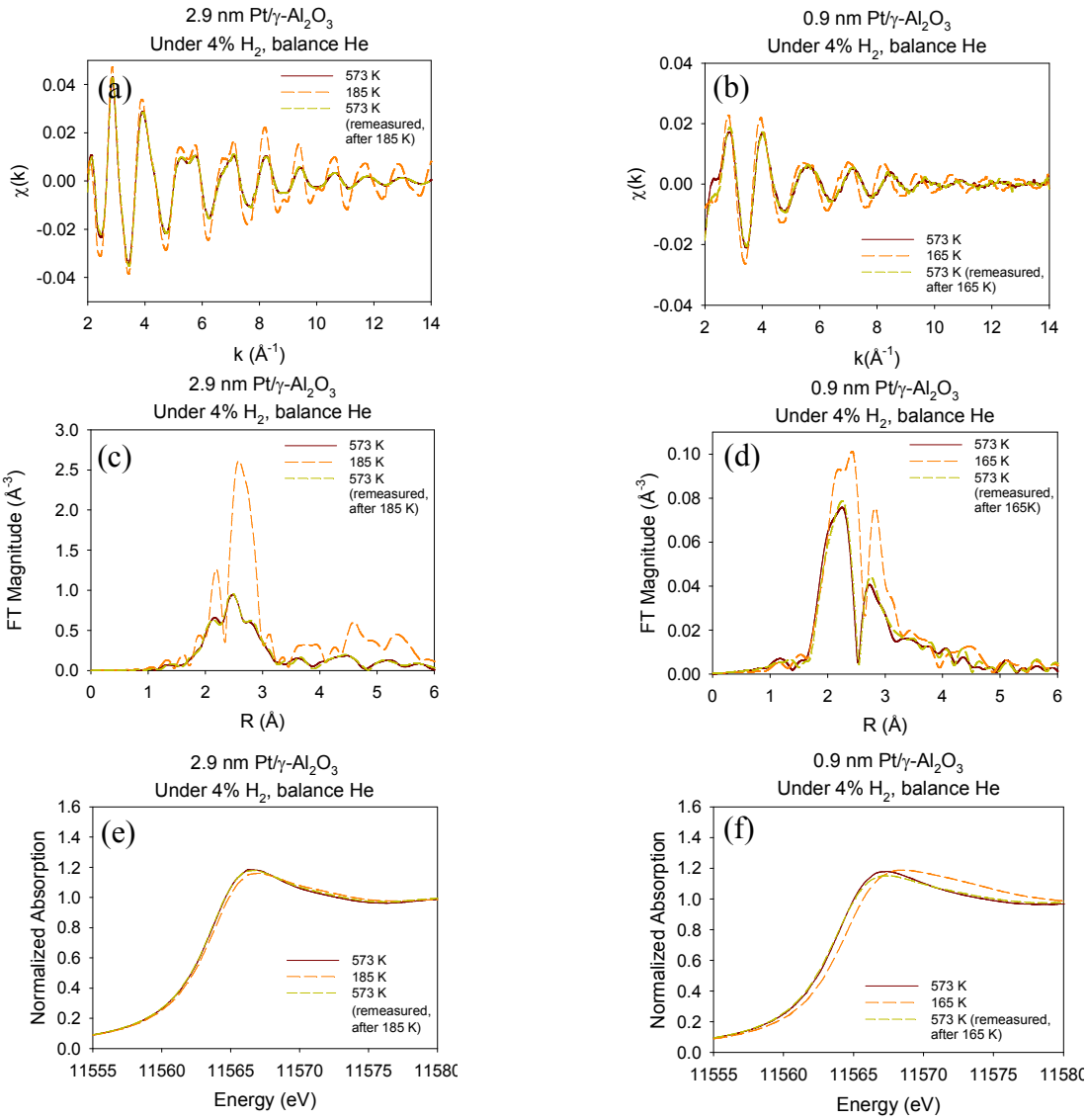

Supporting Information Figure 2.

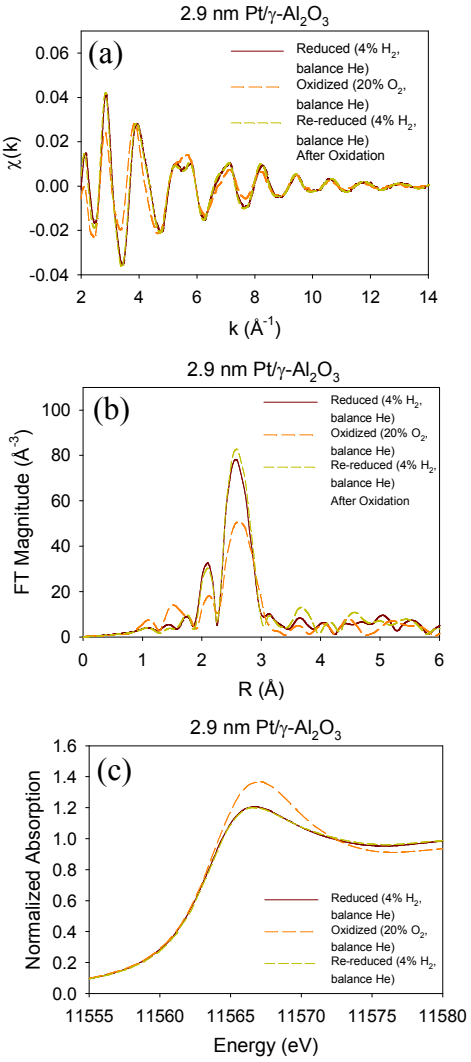

Supporting Information Figure 3.

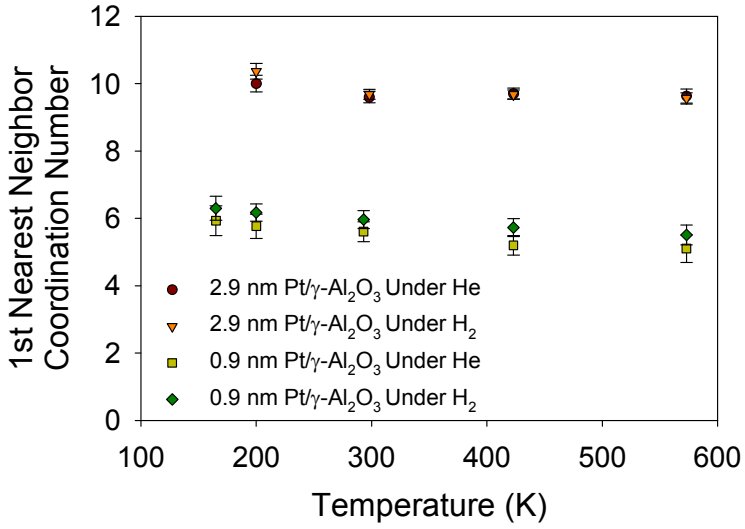

Supporting Information Figure 4.

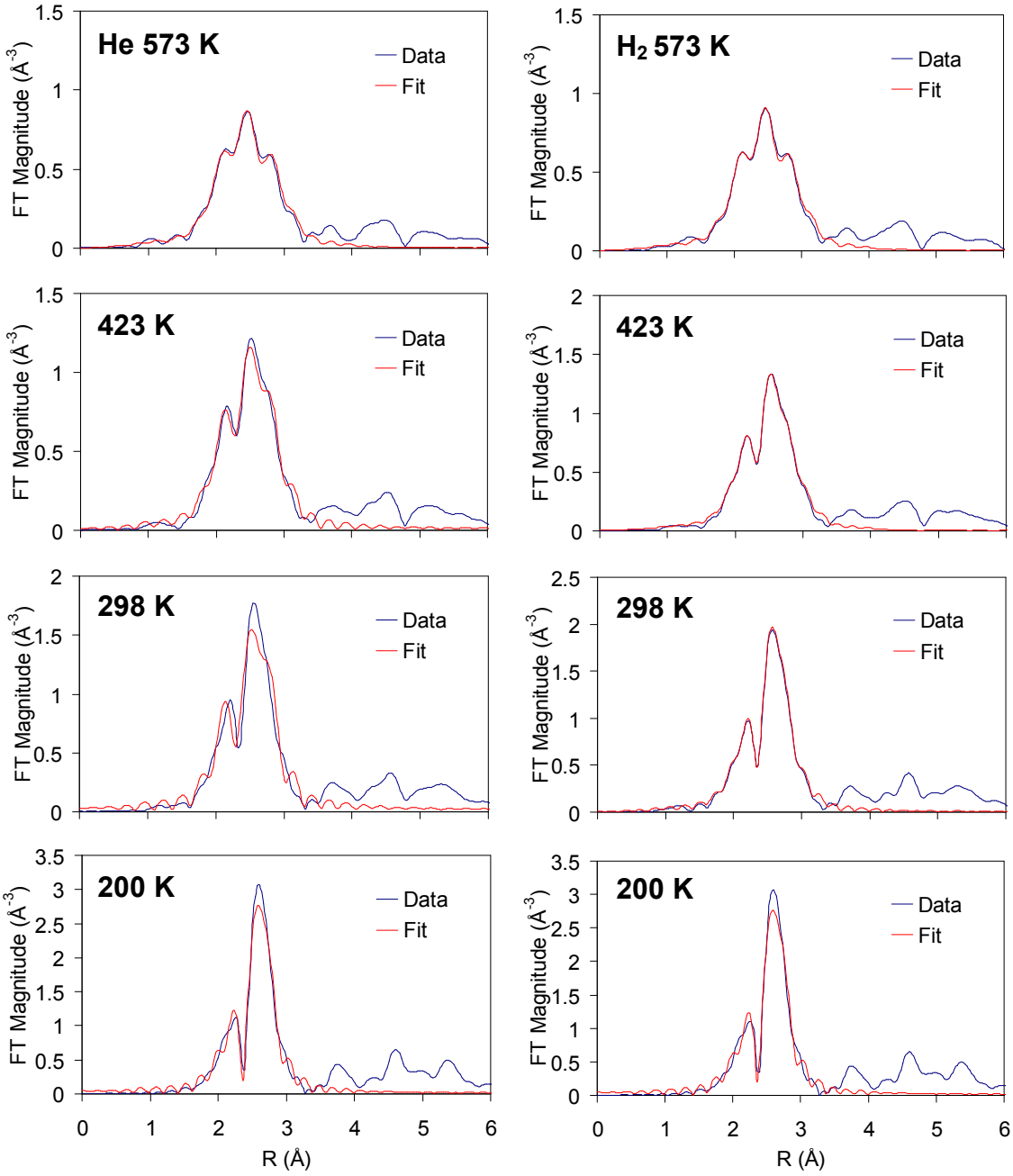

Supporting Information Figure 5.

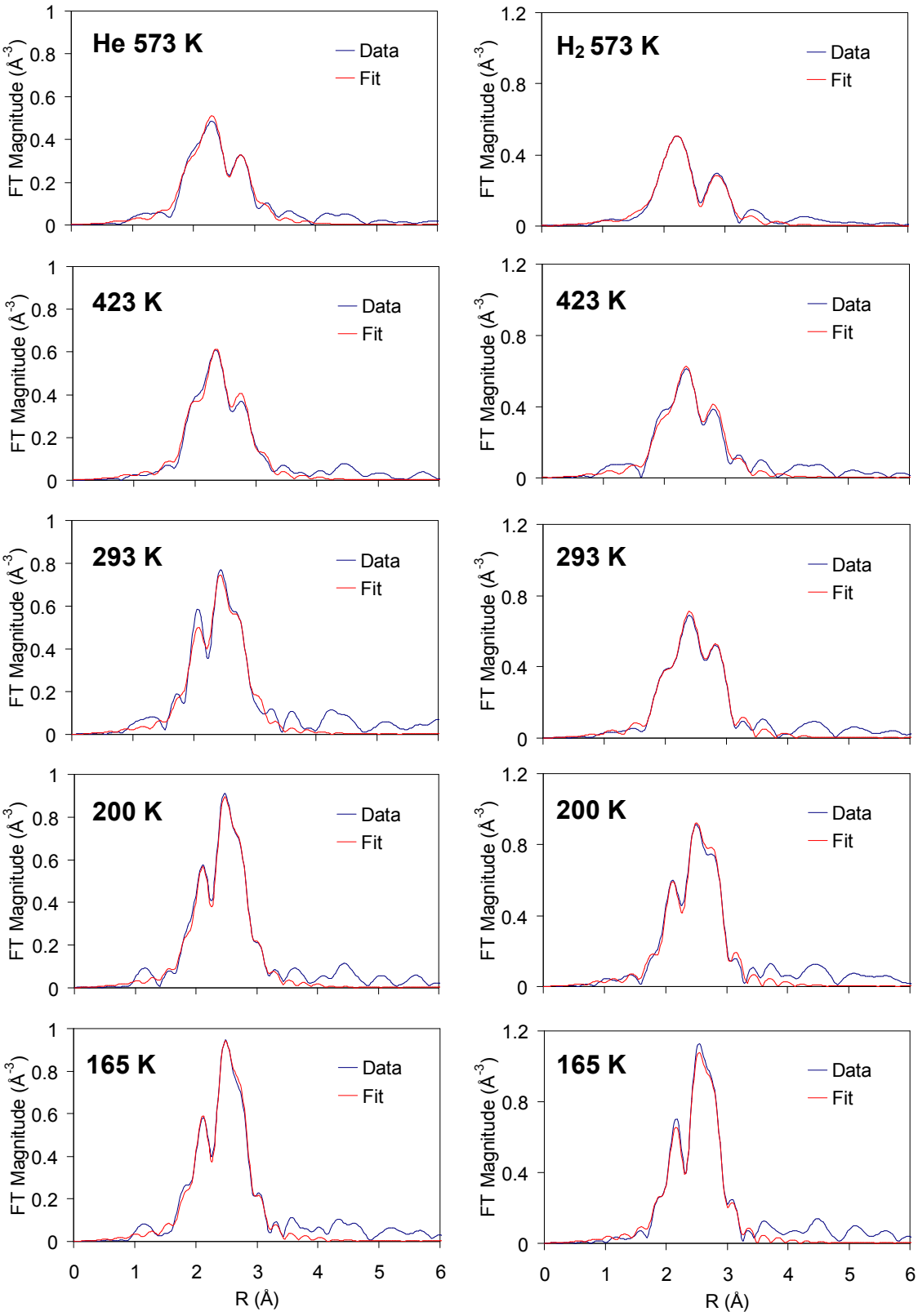

Supporting Information Figure 6.

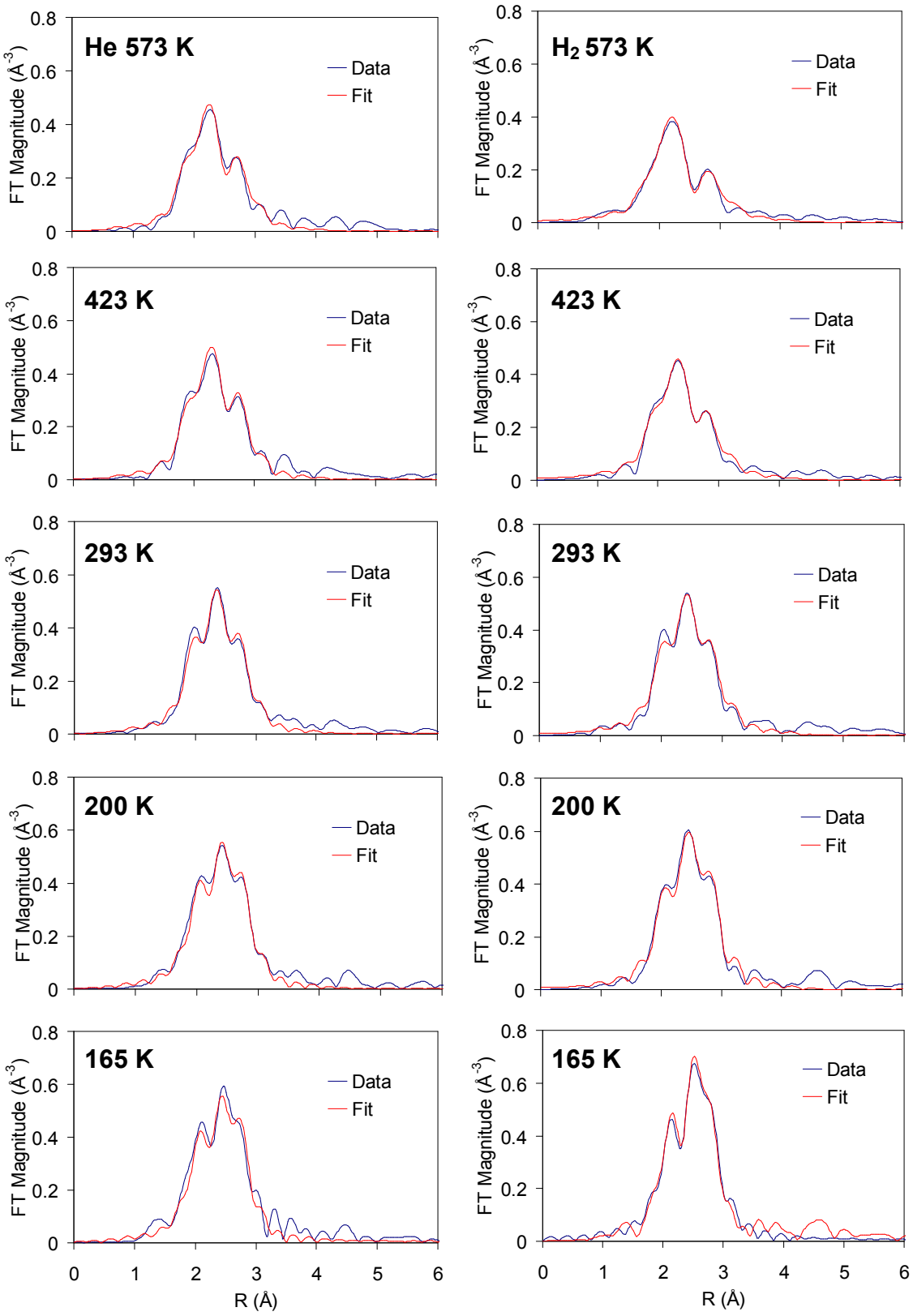

Supporting Information Figure 7.

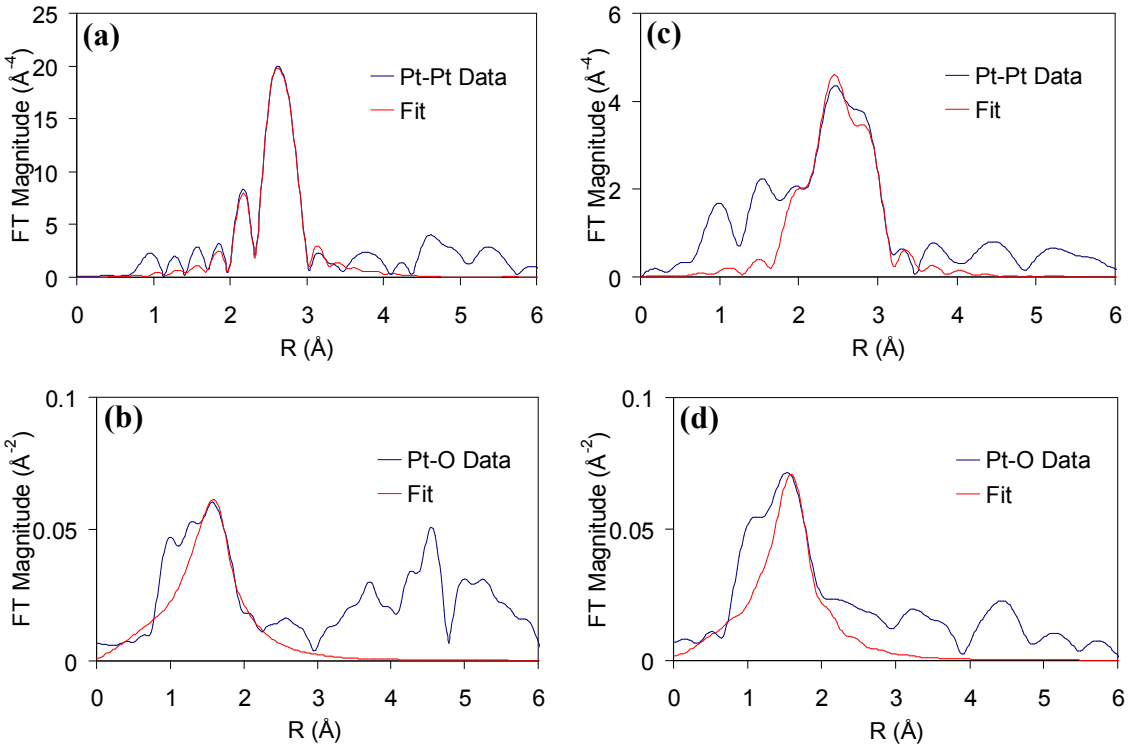

Supporting Information Figure 8.

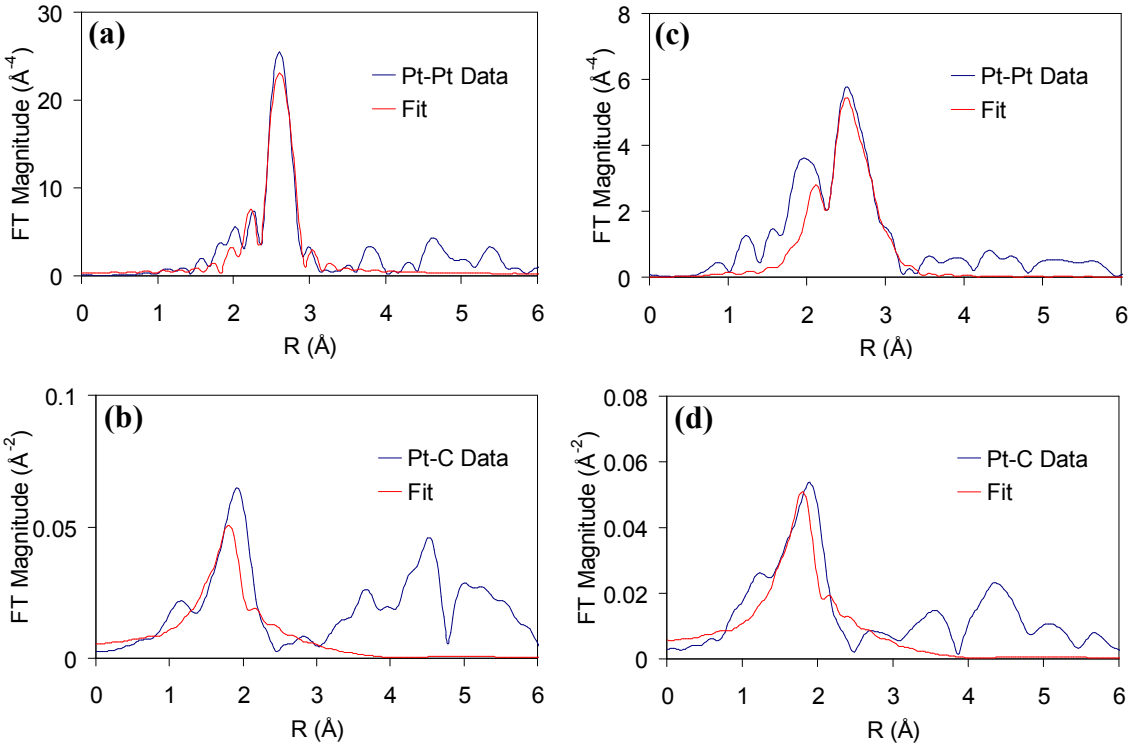

Supporting Information Figure 9.

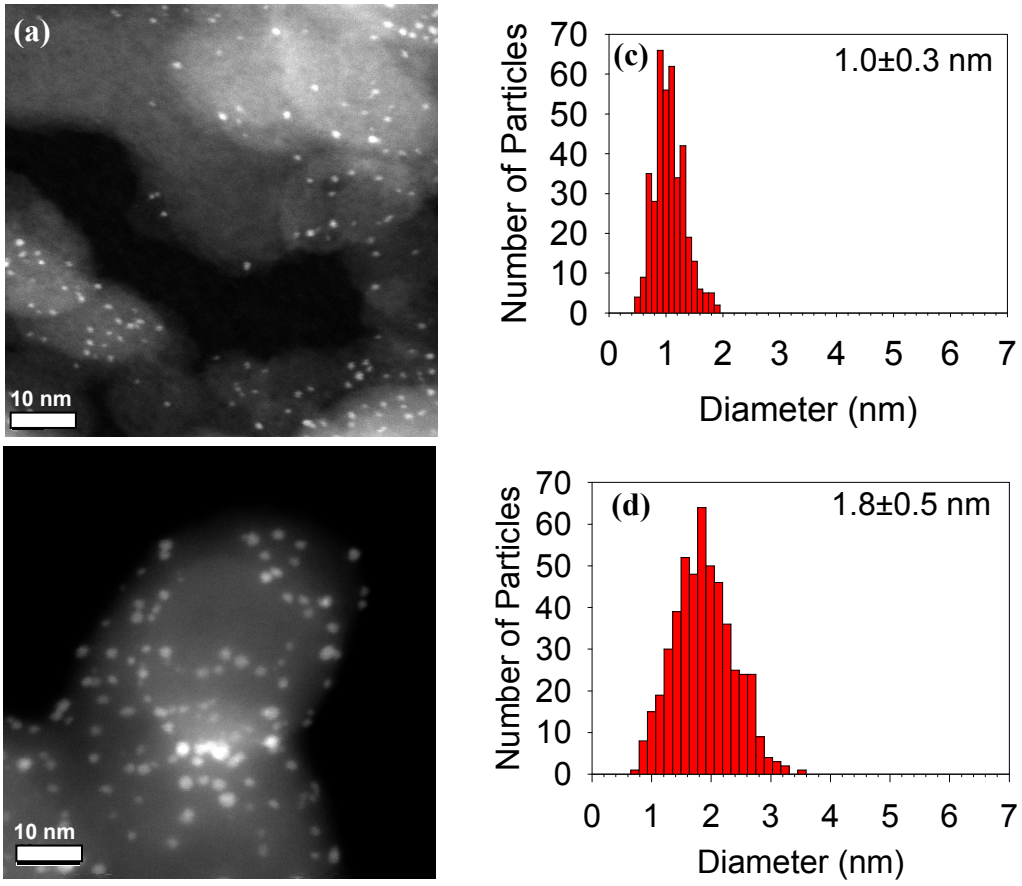

Supporting Information Figure 10.

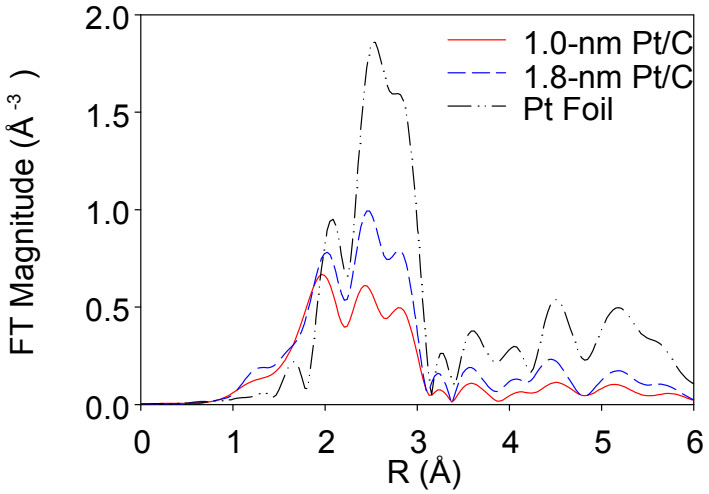

Supporting Information Figure 11.

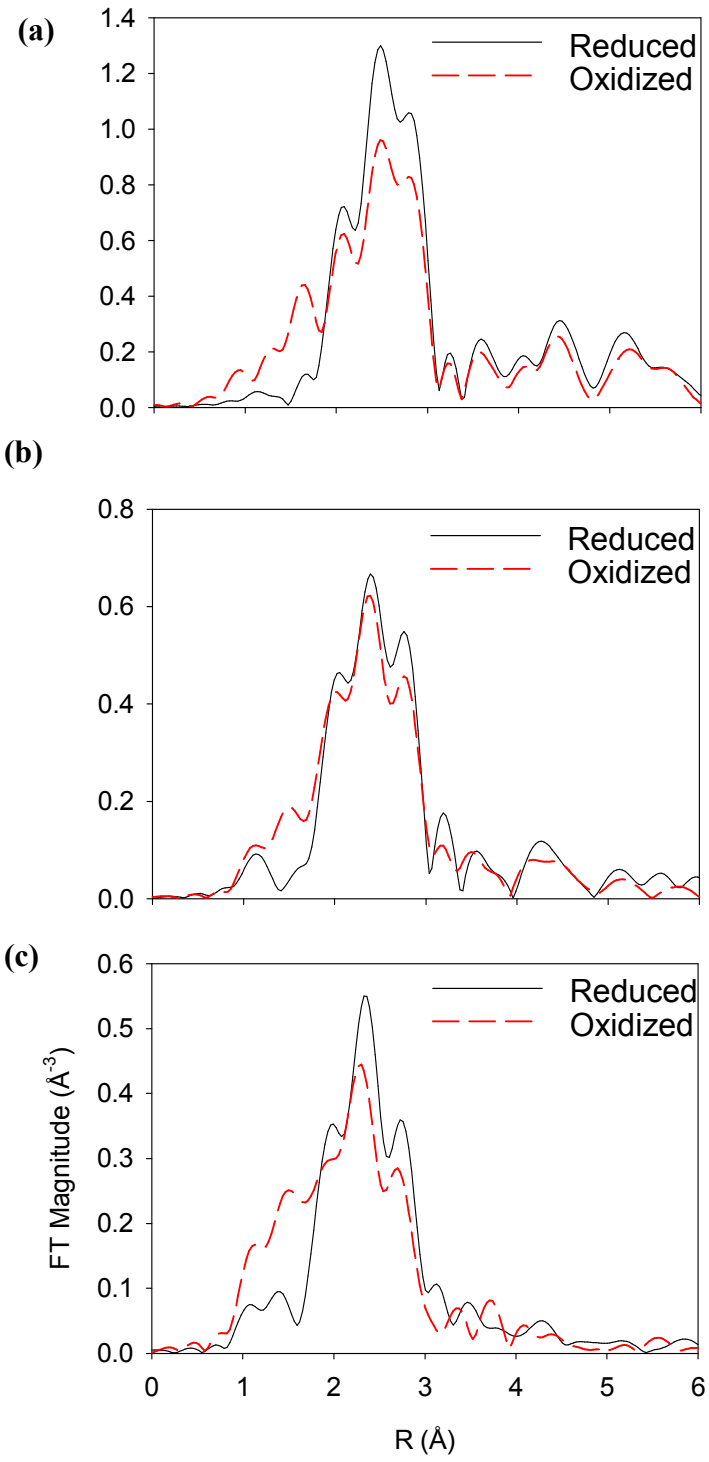

Supporting Information Figure 12.

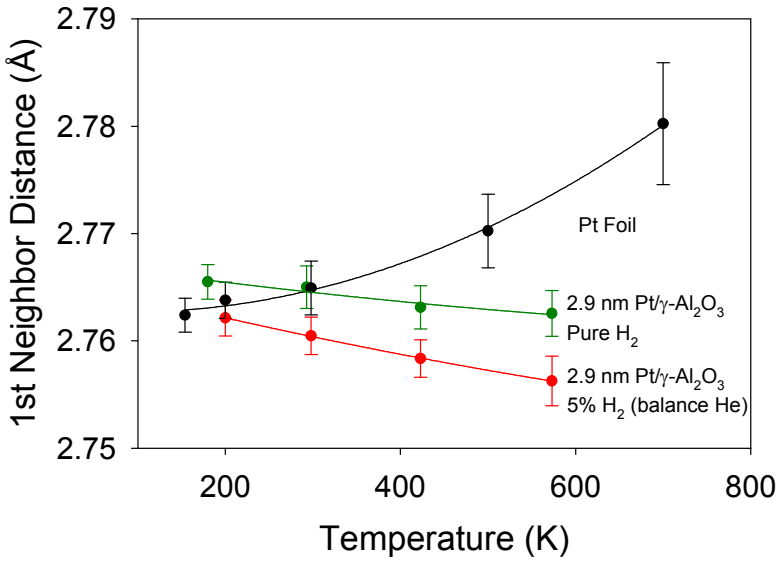

Supporting Information Figure 13.

0.9 nm $\sigma^{(3)}$ values (Å^3)			
Temperature	Atmosphere		
(K)	He	H_2	O_2
165	0.0000(1)	0.0000(1)	N/A
186	N/A	N/A	-0.0001(1)
200	0.0000(1)	0.0001(1)	N/A
215	N/A	N/A	0.0000(1)
293	0.0003(1)	0.0002(1)	0.0003(1)
423	0.0004(1)	0.0005(1)	0.0004(1)
523	N/A	N/A	0.0005(2)
573	0.0006(2)	0.0011(2)	0.0002(2)

1.1 nm $\sigma^{(3)}$ values (Å^3)			
Temperature	Atmosphere		
(K)	He	H_2	O_2
165	0.00006(5)	-0.00002(4)	N/A
177	N/A	N/A	-0.0003(1)
200	0.00006(5)	-0.00001(5)	N/A
216	N/A	N/A	-0.00001(9)
293	0.00012(6)	0.00010(8)	-0.0000(1)
423	0.0004(1)	0.00035(9)	0.0003(1)
523	N/A	N/A	0.0006(2)
573	0.0003(1)	0.0007(2)	0.0006(2)

2.9 nm $\sigma^{(3)}$ values (Å^3)			
Temperature	Atmosphere		
(K)	He	H_2	O_2
186	N/A	N/A	-0.00004(3)
200	0.00000(1)	0.00001(1)	N/A
218	N/A	N/A	-0.00002(3)
293	N/A	N/A	-0.00004(7)
298	0.00002(2)	0.00003(1)	N/A
423	0.00006(2)	0.00009(2)	0.00001(8)
573	0.00014(3)	0.00016(3)	0.0001(1)

1.0 nm $\sigma^{(3)}$ values (Å^3) for Pt/C		
Temperature	Atmosphere	
(K)	He	H_2
170	-0.00007(4)	-0.00004(4)
210	-0.00011(4)	-0.00007(6)
293	-0.00007(6)	0.00005(6)
423	0.00013(8)	0.00010(8)
573	0.0001(1)	0.0002(1)

1.8 nm $\sigma^{(3)}$ values (Å^3) for Pt/C		
Temperature	Atmosphere	
(K)	He	H_2
170	0.00001(1)	0.00001(2)
190	N/A	0.00002(2)
200	0.00001(2)	N/A
293	0.00004(3)	0.00005(3)
423	0.00013(3)	0.00014(4)
573	0.00028(5)	0.00031(7)

Supporting Information Table 1.